AD-A153 835 RAPID ELECTRON BEAM ACCELERATORS (REBA-TRONS)(U) NAVAL RESEARCH LAB WASHINGTON DC C A KAPETANAKOS ET AL. 25 APR 85 NRL-MR-5503 1/1

UNCLASSIFIED F/G 20/7 NL

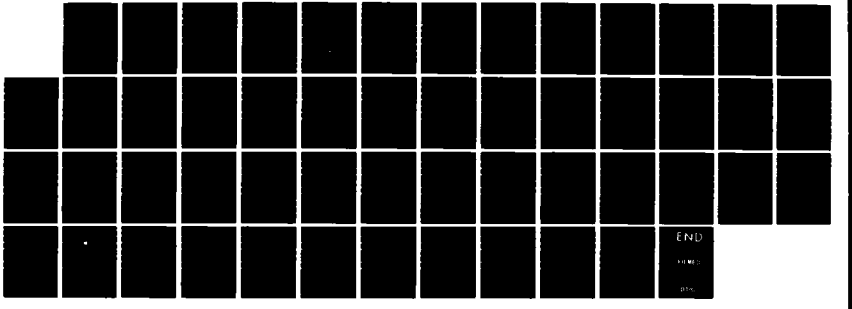

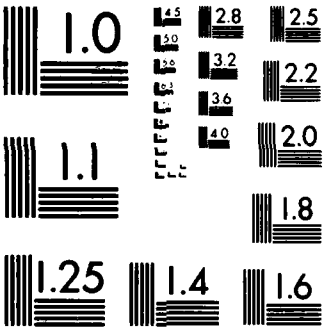

MICROCOPY RESOLUTION TEST CHART
NATIONAL BUREAU OF STANDARDS-1963-A

(2)

NRL Memorandum Report 5503

Rapid Electron Beam Accelerators (REBA-TRONS)

C. A. KAPETANAKOS, P. SPRANGLE, S. J. MARSH,*
D. DIALETIS,† C. AGRITELLIS,† AND A. PRAKASH,‡

Advanced Accelerator Program
Plasma Physics Division

**Sachs/Freeman Associates*
Bowie, MD 20715

†*Science Applications International Corp.*
McLean, VA 22102

‡ *Ballistic Research Laboratory*
Aberdeen, MD 21005

April 25, 1985

This work was supported by the Office of Naval Research
and the U.S. Army Ballistic Research Laboratory.

NAVAL RESEARCH LABORATORY
Washington, D.C.

SECURITY CLASSIFICATION OF THIS PAGE

REPORT DOCUMENTATION PAGE

1a REPORT SECURITY CLASSIFICATION UNCLASSIFIED	1b RESTRICTIVE MARKINGS
2a SECURITY CLASSIFICATION AUTHORITY	3 DISTRIBUTION / AVAILABILITY OF REPORT Approved for public release; distribution unlimited.
2b DECLASSIFICATION / DOWNGRADING SCHEDULE	
4 PERFORMING ORGANIZATION REPORT NUMBER(S) NRL Memorandum Report 5503	5 MONITORING ORGANIZATION REPORT NUMBER(S)
6a NAME OF PERFORMING ORGANIZATION Naval Research Laboratory 6b OFFICE SYMBOL (If applicable) Code 4704	7a NAME OF MONITORING ORGANIZATION Office of Naval Research
6c ADDRESS (City, State, and ZIP Code) Washington, DC 20375-5000	7b ADDRESS (City, State, and ZIP Code) Arlington, VA 22217
8a NAME OF FUNDING / SPONSORING ORGANIZATION ONR and BRL 8b OFFICE SYMBOL (If applicable)	9 PROCUREMENT INSTRUMENT IDENTIFICATION NUMBER
8c ADDRESS (City, State, and ZIP Code) Arlington, VA 22217 Aberdeen, MD 21005	10 SOURCE OF FUNDING NUMBERS PROGRAM ELEMENT NO: 61153N; PROJECT NO.: ; TASK NO.: RR011-09-4E; WORK UNIT ACCESSION NO.: DN180-207

11 TITLE (Include Security Classification)

Rapid Electron Beam Accelerators (REBA-TRONS)

12 PERSONAL AUTHOR(S)

Kapetanakos, C.A., Sprangle, P., Marsh, S.J.,* Dialetis, D.,† Agritellis, C.,† and Prakash, A.‡

13a TYPE OF REPORT	13b TIME COVERED	14 DATE OF REPORT (Year, Month, Day)	15 PAGE COUNT
Interim	FROM _____ TO _____	1985 April 25	55

16 SUPPLEMENTARY NOTATION *Sachs/Freeman Associates, Bowie, MD 20715

†Science Applications International Corp., McLean, VA 22102 (Continues)

17 COSATI CODES			18 SUBJECT TERMS (Continue on reverse if necessary and identify by block number)
FIELD	GROUP	SUB-GROUP	

19 ABSTRACT (Continue on reverse if necessary and identify by block number)

We have carried out an extensive numerical and analytical investigation of the beam dynamics in a rebatron accelerator. In this device acceleration occurs by a localized, high gradient electric field and beam confinement is achieved by a strong focusing torsatron magnetic field. In a rebatron, beam acceleration occurs in a few microseconds and limitations imposed by instabilities, field errors and radiation losses can be relaxed. Our studies indicate that both the bandwidth and the maximum electron beam current than can be confined by these devices is remarkably high.

20 DISTRIBUTION / AVAILABILITY OF ABSTRACT	21 ABSTRACT SECURITY CLASSIFICATION
☒ UNCLASSIFIED/UNLIMITED ☐ SAME AS RPT ☐ DTIC USERS	UNCLASSIFIED
22a NAME OF RESPONSIBLE INDIVIDUAL C. A. Kapetanakos	22b TELEPHONE (Include Area Code) (202) 767-2838 22c OFFICE SYMBOL Code 4704

DD FORM 1473, 84 MAR 83 APR edition may be used until exhausted
All other editions are obsolete

SECURITY CLASSIFICATION OF THIS PAGE

16. SUPPLEMENTARY NOTATION (Continued)

‡Ballistic Research Laboratory, Aberdeen, MD 21005

This work was supported by the Office of Naval Research and the U.S. Army Ballistic Research Laboratory.

CONTENTS

RAPID ELECTRON BEAM ACCELERATORS (REBA-TRONS)

I. Introduction

Ultra-high current accelerators are rapidly becoming an active area of research.[1,2] The development of these devices is mainly motivated by a variety of potential applications[1,3,4] that are extended over several areas, including environment, food processing, radiation sources, x-ray radiography and national defense.

Among the various accelerating schemes that have the potential to produce ultra-high power electron beams, induction accelerators[1,2] appear to be the most promising. Induction accelerators are inherently low impedance devices and thus are ideally suited to drive high current beams. The acceleration process is based on the inductive electric field produced by a time varying magnetic field.

Quite naturally, induction accelerators are divided into linear[5-13] and cyclic[14-19] devices. In linear devices the accelerating field is localized in the gap, while in their cyclic counterparts the electric field is continuous along the orbit of the accelerated particles. Both cyclic and linear devices require the same total magnetic flux change to achieve a given energy increment. However, in linear accelerators the total change of flux occurs in one transit time, typically in less than 100 nsec, while in cyclic accelerators the same change occurs over several thousand revolutions in a typical time of one msec.

As a consequence of the slow acceleration, the accelerated beam must be confined by the focusing magnetic field over long periods of time and thus field errors, instabilities and radiation losses impose limitations on the cyclic accelerators. These limitations can be substantially relaxed if the acceleration could occur rapidly as in

Manuscript approved February 7, 1985.

linear accelerators. Therefore, a device that combines the rapid acceleration of linear accelerators and the compact size of cyclic accelerators is highly desirable. In this paper, we propose such a hybrid scheme that combines most of the advantages of linear and cyclic accelerators. This device has been named REBA-TRON (Rapid Electron Beam Accelerator). The rebatron is similar to the racetrack induction accelerator.[20]

A rebatron is shown schematically in Fig. 1. The high gradient localized field that is responsible for the rapid acceleration is produced by convoluted parallel transmission lines, although, other transmission lines may be more appropriate in an actual system. Since the acceleration occurs over a few μsec, the constraints imposed on the vertical field are very stringent. In an actual device the vertical field is generated by two coaxial, cylindrical plates that carry current in the opposite direction. The axes of these lines coincide with the major axis of the toroidal vessel and they are located symmetrically around the minor axis of the torus. These transmission lines change mainly the local, vertical magnetic field, while the magnetic flux through the beam orbit remains approximately constant. The mismatch between the beam energy and the vertical field is alleviated by a strong focusing field. This field is generated by a set of $\ell = 2$ torsatron windings, i.e., two twisted wires that carry current in the same direction. In addition to the transverse components of the field, the torsatron windings provide a zero order toroidal magnetic field. The purpose of the resistive chamber wall is to facilitate the beam trapping[21] in the applied magnetic field. Beam capture in the rebatrons is very difficult, because the strong focusing field makes the particle orbit insensitive to the energy mismatch and thus small changes

in the betatron (vertical) magnetic field are not sufficient to move the beam from the injection position near the wall to the minor axis of the torus.

The superior confining properties of twisted quadruple fields have been recognized for several years.[22] Recently, it has been reported[19] that the ℓ=2 Stellarator configuration has an energy bandwidth of ~50%.

In this report, we are presenting results from our studies of the beam dynamics in a rebatron accelerator when the magnetic fields are not a function of time. In addition, the local vertical magnetic field has been replaced by a betatron magnetic field. Our results indicate that both the bandwidth and the maximum electron current that can be confined by a rebatron are very high. Results with the local, fast varying vertical field will be reported in a forthcoming publication.

II. The Applied Fields

a. Magnetic Fields

In the local cyclindrical coordinate system $\hat{e}_\rho$, $\hat{e}_\phi$, $\hat{e}_s$ shown in Fig. 2, the magnetic field components of the $\ell = 2$ torsatron are given by

$$B_\rho = B_\rho^{(o)} + B_{\rho+}^{(1)} + B_{\rho-}^{(1)} , \tag{1a}$$

$$B_\phi = B_\phi^{(o)} + B_{\phi+}^{(1)} + B_{\phi-}^{(1)} , \tag{1b}$$

$$B_s = \frac{1}{1 + (\rho / r_o) \cos \phi} \left[B_s^{(o)} + B_{s+}^{(1)} + B_{s-}^{(1)} \right] , \tag{1c}$$

components in the numerical integration of the orbit equations. It has been determined that the first two non zero terms in the expansion are sufficient to describe the field in the region $\rho/a \leq 0.5$ with an accuracy better than 95%.

In the analytical work described in Section IV, the toroidal corrections have been neglected as well as all the terms with $m > 2$. Furthermore, it has been assumed that $\hat{\kappa} \ll 1$. Under these simplifications the torsatron magnetic field becomes

$$B_\rho \simeq 2B_s^{ex}\varepsilon_t I_2'(x) \sin [2(\phi - \alpha s)], \tag{9}$$

$$B_\phi \simeq \frac{4B_s^{ex}}{x} \varepsilon_t I_2(x) \cos [2(\phi - \alpha s)], \tag{10}$$

$$B_s \simeq B_o - 2B_s^{ex}\varepsilon_t I_2(x) \cos [2(\phi - \alpha s)], \tag{11}$$

where $B_s^{ex}\varepsilon_t = B_o x_o K_2'(x_o)$.

For $x \ll 1$, Eqs. (9), (10) and (11) become

$$B_\rho \simeq \frac{B_s^{ex}\varepsilon_t x}{2} \sin [2(\phi - \alpha s)], \tag{12}$$

$$B_\phi \simeq \frac{B_s^{ex}\varepsilon_t x}{2} \cos [2(\phi - \alpha s)], \tag{13}$$

$$B_s \simeq B_o . \tag{14}$$

In addition to the torsatron field, the rebatron accelerator includes a betatron or vertical magnetic field and a toroidal field, B_s^{ex}, that is produced by a set of toroidal coils. The two

components of the betatron field are described by the linearized equations

$$B_z \approx B_{zo}\,[1-n\,x/r_o], \tag{15}$$

$$B_r \approx -\,B_{zo}\,ny/r_o, \tag{16}$$

where B_{zo} is the betatron field at the reference orbit, i.e., at $x = y = 0$ and n is the external field index.

The toroidal field produced by a set of toroidal coils is independent of toroidal angle and therefore varies as 1/r. This toroidal field can be chosen to have either the same or opposite polarity to the torsatron toroidal field.

b. The Electric Field in the Gap

Consider two cylinders with their axes lying along the same line and separated by a distance d as shown in Fig. 4a. Since the cylinder on the left is charged to $-V_o$ and the cylinder to the right is charged to $+V_o$ the average electric field in the gap is $\langle E_s \rangle = 2\,V_o/d$. The local electric field is given by the solution of Laplace equation, i.e., $\nabla^2 \Phi = 0$. For $|s| > d/2$, the exact components of the electric field are:

$$E_s = -\frac{4V_o}{d} \sum_{n=1}^{\infty} \frac{\sinh(\lambda_n d/2) J_o(\lambda_n \rho)\, e^{-\lambda_n |s|}}{\lambda_n a J_1(\lambda_n a)}\,, \tag{17}$$

$$E_\rho = -\frac{s}{|s|}\,\frac{4V_o}{d} \sum_{n=1}^{\infty} \frac{\sinh(\lambda_n d/2) J_1(\lambda_n \rho)\, e^{-\lambda_n |s|}}{\lambda_n a J_1(\lambda_n a)}\,. \tag{18}$$

Similarly, for $|s| < d/2$, the two components of the electric field are:

$$E_s = -\frac{4V_o}{d}\left[\frac{1}{2} - \sum_{n=1}^{\infty} \frac{J_o(\lambda_n \rho)e^{-\lambda_n d/2}\cosh(\lambda_n s)}{a\lambda_n J_1(\lambda_n a)}\right], \qquad (19)$$

and

$$E_\rho = -\frac{4V_o}{d}\sum_{n=1}^{\infty} \frac{J_1(\lambda_n \rho)e^{-\lambda_n d/2}\sinh(\lambda_n s)}{\lambda_n a J_1(\lambda_n a)}, \qquad (20)$$

where $J_o(\lambda_n a) = 0$, a is the radius of the cylinders and J_o and J_1 are the Bessel functions.

The electric field lines that correspond to the field components given by Eqs. (17) to (20) are plotted in Fig. 4b. These electric fields are a good representation of the fields produced inside the torus by a transmission line, since in this region the inductive magnetic field is zero and therefore the potential is described by $\nabla^2\phi = 0$.

III. Numerical Results

To investigate the confining properties of the torsatron magnetic field, we have integrated the relativistic equations of motion using Eqs. (1) to (7) for the torsatron magnetic field and Eqs. (15) and (16) for the betatron field. The accelerating gap is 2 cm wide and as shown in Fig. 5, the electric field is limited to a 0.60 radian wide toroidal sector. For reasons that are discussed later on, the self fields have been omitted in these runs.

In the first run, the current in the torsatron windings is chosen

to be zero. Figure 6a shows the normalized particle energy (γ) as a function of time and Fig. 6b the projection of the particle orbit in the transverse plane. The various parameters for this run are listed in Table II. Since ε_t is zero, the magnetic field configuration is that of the modified betatron. As a consequence of the curvature drift, the gyrating particle drifts out of the system in about 26 nsec, i.e., in about a revolution around the major axis. As expected, the guiding center of the particle moves mainly in the vertical direction, while the particle gyrates around its guiding center with a frequency corresponding to the local toroidal field.

Figures 7a and 7b show the normalized energy of the particle and its orbit when approximately -124.7 kA of current flows through the torsatron windings. The rest of the parameters for this run are listed in Table III. The particle remains confined for eight revolutions. Figures 8a and 8b show similar results when the current in the windings is increased to approximately -250 kA. The corresponding torsatron field strength factor ε_t is -0.8. The remainder of the parameters are listed in Table IV. In all three runs the betatron magnetic field was held constant at 118 G. These results clearly demonstrate that the confining properties of the system are substantially improved by the addition of the torsatron field. The particle strikes the chamber wall when its gamma approaches approximately 65. The total time the particle remains in the system is about 320 nsec, i.e., more than an order of magnitude longer than when the torsatron field is absent.

Further improvement in the particle confinement is observed when the period of the windings is reduced or the current in the windings increased. An additional modest improvement in the confinement of the

system is observed when the betatron field is increased above its matching value. This is shown in Fig. 9. The betatron field for this run is 236 G and the remainder of the parameters are identical to those in Fig. 8. The confinement time increased by 20 nsec, i.e., from 320 to 340 nsec. However, when the betatron field increased to 472 G the confinement time was reduced to 290 nsec.

IV. Theoretical Model

To gain a better understanding of the focusing properties of the torsatron fields, we have developed a theoretical model that is based on linear external fields. Obviously, these fields are appropriate only near the minor axis of the torus, i.e., when $2\alpha\rho \ll 1$.

The components of the torsatron field in the coordinate system $\hat{e}_r$, $\hat{e}_\theta$, $\hat{e}_z$ shown in Fig. 2 are

$$B_{rt} = B_\rho \cos\phi - B_\phi \sin\phi = B_s^{ex} \varepsilon_t \alpha \left[z\cos 2\alpha r_o^\theta + (r-r_o) \sin 2\alpha r_o^\theta \right], \quad (21)$$

$$B_{zt} = B_\rho \sin\phi + B_\phi \cos\phi = B_s^{ex} \varepsilon_t \alpha \left[(r-r_o)\cos 2\alpha r_o^\theta - z \sin 2\alpha r_o^\theta \right], \quad (22)$$

$$B_{\theta t} = - B_o, \quad (23)$$

where $- r_o^\theta = s$.

In addition, the betatron magnetic field is given by

$$B_{zb} \simeq B_{zo} \left[1 - \frac{n(r-r_o)}{r_o} \right], \quad (24)$$

and

$$B_{rb} \simeq - nB_{zo}\, z/r_o, \tag{25}$$

where n is the external field index. The total field components are

$$B_r = B_{rt} + B_{rb}, \tag{26}$$

$$B_z = B_{zt} + B_{zb}, \tag{27}$$

$$B_\theta = B_{\theta t} - B_s^{ex}, \tag{28}$$

where B_s^{ex} indicates any additional toroidal field that may be applied.

The accelerating electric field components are approximated by

$$E_r \simeq \frac{(r-r_o)}{2r_o}\, \ddot{\gamma} \left(\frac{mc^2}{e}\, \frac{r_o}{v_\theta^2}\right), \tag{29}$$

$$E_z \simeq \frac{z}{2r_o}\, \ddot{\gamma} \left(\frac{mc^2}{e}\, \frac{r_o}{v_\theta^2}\right), \tag{30}$$

$$E_\theta \simeq - \frac{mc^2}{ev_\theta}\, \dot{\gamma}, \tag{31}$$

where $\dot{\gamma} = d\gamma/dt$, $\ddot{\gamma} = d^2\gamma/dt^2$ and v_θ is the toroidal velocity, which is assumed constant.

Using Eqs. (26) to (31) for the fields, the equations of motion in the laboratory frame become

$$\ddot{R} + \omega_R^2 R + \frac{\omega_o \omega_w}{2} \left(R\cos\omega_w t - Z\sin\omega_w t\right) - \left(\dot{Z} - \frac{\dot{\gamma}}{2\gamma} Z\right) \frac{\Omega_\theta}{\gamma} = \lambda^2(t), \tag{32}$$

$$\ddot{Z} + \omega_z^2 Z - \frac{\omega_o \omega_w}{2}\left(Z\cos\omega_w t + R\sin\omega_w t\right) + \left(\dot{R} - \frac{\dot{\gamma}}{2\gamma} R\right)\frac{\Omega_A}{\gamma} = 0 \ , \qquad (33)$$

where

$$R = \gamma^{1/2}(r-r_o), \quad Z = \gamma^{1/2} z \ ,$$

$$\Omega_A = eB_A/mc \ , \qquad \Omega_{zo} = eB_{zo}/mc \ ,$$

$$\omega_o = \Omega_s^{ex} \varepsilon_t/\gamma \ , \qquad \omega_w = 2\alpha v_A \ ,$$

$$\lambda^2(t) = \frac{c^2}{r_o}\gamma^{1/2}\frac{v_A}{c}\left(\frac{v_A}{c} - \frac{r_o \Omega_{zo}}{c\gamma}\right) \ ,$$

$$\omega_R^2 = 1/4\left(\frac{\dot{\gamma}}{\gamma}\right)^2 - 1/2\left(\frac{\ddot{\gamma}}{\gamma}\right) + \frac{\ddot{\gamma}}{\gamma}\left(\frac{c^2}{2v_A^2}\right) - \frac{v_A \Omega_{zo}}{\gamma}\frac{n}{r_o} + \frac{v_A^2}{r_o^2} \ ,$$

and

$$\omega_z^2 = 1/4\left(\frac{\ddot{\gamma}}{\gamma}\right)^2 - 1/2\left(\frac{\ddot{\gamma}}{\gamma}\right) + \frac{\ddot{\gamma}}{\gamma}\left(\frac{c^2}{2v_A^2}\right) + \frac{v_A \Omega_{zo} n}{\gamma r_o} \ .$$

Equations (32) and (33) become more tractable when transformed to a frame rotating with angular frequency $\omega_w/2$. Using the transformation

$$R = \tilde{R}\cos\left(\frac{\omega_w t}{2}\right) + \tilde{Z}\sin\left(\frac{\omega_w t}{2}\right), \qquad (34)$$

$$Z = -\tilde{R}\sin\left(\frac{\omega_w t}{2}\right) + \tilde{Z}\cos\left(\frac{\omega_w t}{2}\right), \qquad (35)$$

equations (32) and (33) become

$$\ddot{\tilde{R}} + \left[\omega_1^2 - \delta\omega^2\cos\omega_w t + \frac{\omega_o\omega_w}{2} - \left(\frac{\omega_w}{2}\right)^2 + \left(\frac{\omega_w}{2}\right)\frac{\Omega_\theta}{\gamma}\right]\tilde{R} +$$

$$\left[\omega_w - \frac{\Omega_\theta}{\gamma}\right)\dot{\tilde{Z}} + \left(\frac{\dot{\gamma}}{2\gamma}\ \frac{\Omega_\theta}{\gamma} - \delta\omega^2\sin\omega_w t\right]\tilde{Z} = \lambda^2\cos\left(\frac{\omega_w t}{2}\right), \qquad (36)$$

$$\ddot{\tilde{Z}} + \left[\omega_1^2 + \delta\omega^2\cos\omega_w t - \frac{\omega_o\omega_w}{2} - \left(\frac{\omega_w}{2}\right)^2 + \left(\frac{\omega_w}{2}\right)\frac{\Omega_\theta}{\gamma}\right]\tilde{Z} -$$

$$\left(\omega_w - \frac{\Omega_\theta}{\gamma}\right)\dot{\tilde{R}} - \left(\frac{\dot{\gamma}}{2\gamma}\ \frac{\Omega_\theta}{\gamma} + \delta\omega^2\sin\omega_w t\right)\tilde{R} = \lambda^2\sin\left(\frac{\omega_w t}{2}\right), \qquad (37)$$

where

$$\omega_1^2 = 1/4\left(\frac{\dot{\gamma}}{\gamma}\right)^2 - 1/2\left(\frac{\ddot{\gamma}}{\gamma}\right) + \frac{\ddot{\gamma}}{\gamma}\left(\frac{c^2}{2v_\theta^2}\right) + \frac{v_\theta^2}{2r_o^2} \simeq 1/4\left(\frac{\dot{\gamma}}{\gamma}\right)^2 + \frac{v_\theta^2}{2r_o^2},$$

and

$$\delta\omega^2 = \frac{v_\theta\, n}{r_o}\left(\frac{\Omega_{zo}}{\gamma} - \frac{v_\theta}{2nr_o}\right)$$

Since at the start of the acceleration $\left|\omega_o\omega_w/2\right| >> \left|\delta\omega^2\right|$ and $(\dot{\gamma}/2\gamma)\left|\left(\frac{\Omega_\theta}{\gamma}\right)\right| >> \left|\delta\omega^2\right|$, the two coupled equations (36) and (37) can be combined into a single equation by introducing the complex variable $\tilde{\psi} = \tilde{R} + i\,\tilde{Z}$. Multiplying Eq. (37) by i and adding it to Eq. (36), it is obtained

$$\ddot{\tilde{\psi}} + f_1\tilde{\psi} + f_3\tilde{\psi}^* - if_2\dot{\tilde{\psi}} = \lambda^2 e^{i\omega_w t/2}, \qquad (38)$$

where

$$f_1 = \omega_1^2 - \left(\frac{\omega_w}{2}\right)^2 + \frac{\omega_w}{2}\frac{\Omega_\theta}{\gamma} - \frac{i\dot{\gamma}}{2\gamma}\frac{\Omega_\theta}{\gamma}\,, \quad f_2 = \left(\omega_w - \frac{\Omega_\theta}{\gamma}\right) \quad \text{and}$$

$$f_3 = \frac{\omega_o \omega_w}{2}\,.$$

Equations (36) and (37) have been solved numerically. After integration the orbit is transferred back to the laboratory frame. The results are shown in Fig. 10. The projection of the orbit in the r,z plane is shown in Fig. 10a, the particle radial distance from the minor axis as a function of time is shown in Fig. 10b and γ as a function of time in Fig. 10c. The various parameters for this run are identical to those listed in Table IV. The particle strikes the wall at about 325 nsec, when its gamma is approximately 68. These results are in good agreement with those of Fig. 8 that have been obtained using the more accurate expressions for the torsatron fields. As will be discussed later, the particle was lost because at $\gamma \approx 65$ it entered the unstable region that extends from $\gamma = 65$ to $\gamma = 121$.

When $\dot{\gamma} = 0$, the homogeneous part of Eq. (38) becomes

$$\ddot{\tilde{\psi}} + [2f_1 + f_2^2]\,\dot{\tilde{\psi}} + [f_1^2 - f_3^2]\,\tilde{\psi} = 0, \tag{39}$$

i.e., a fourth order equation with constant coefficients. The solutions of Eq. (39) are of the type $\tilde{\psi} = \tilde{\psi}_o\, e^{i\omega t}$, where ω^2 , is given by

$$\omega_\pm^2 = 1/4\left(\omega_w - \frac{\Omega_\theta}{\gamma}\right)^2 + \frac{\Omega_\theta^2}{4\gamma^2} \pm \frac{\Omega_\theta}{2\gamma}\left[\left(\omega_w - \frac{\Omega_\theta}{\gamma}\right)^2 + \omega_w^2 \varepsilon_t^2 \left(\frac{\Omega_s^{ex}}{\Omega_\theta}\right)^2\right]^{1/2}, \tag{40}$$

when $|\omega_1^2| \ll |\omega_o \omega_w/2|$.

The particle orbits are stable when ω is real, i.e., when

$$\mu(\gamma) \equiv \left(\Omega_\theta - \frac{\omega_w \gamma}{2}\right)^2 - \varepsilon_t^2 \, \Omega_s^{ex^2} > 0. \tag{41}$$

The two roots of (40) are given by

$$\gamma_\pm = \frac{2\Omega_\theta}{\omega_w} \left(1 \pm \varepsilon_t \frac{\Omega_s^{ex}}{\Omega_\theta}\right) . \tag{42}$$

The function $\mu(\gamma)$ is plotted in Fig. 11 for three values of B_θ and B_s^{ex}. In Fig. 11a $B_s^{ex} = -6kG$, $B_o = 5KG$ and thus $B_\theta = -(B_s^{ex} + B_0) = 1KG$. For this value of toroidal magnetic field and for $\varepsilon_t = 0.4$ and $\omega_w/2 = 3\times10^9$ sec^{-1}, Eq. (42) gives 19.96 and -8.2 for the two roots of Eq. (41). Therefore, at $\gamma = 7$ the particle orbit should be unstable. Results from the numerical integration of nonlinear orbit equations for $\dot{\gamma} = 0$, and $\gamma = 7$ and using the same values for the rest of the parameters as in Fig 11a are shown in Fig. 12. As expected, the orbit is indeed unstable and the particle is lost in less than one nsec.

By reversing the direction of the current in the torsatron wires B_o and ε_t change sign and the two roots of Eq. (41) become 50.5 and 78.7. Therefore, for $\gamma = 7$ the orbit is stable. This is in agreement with the results from the numerical integration of nonlinear orbit equations shown in Fig. 13.

When $\gamma_\pm < 1$, the orbits are stable for all values of γ . For

$B_s^{ex} = 6KG$, $B_o = 5KG$ and $\varepsilon_t = -0.4$ the two roots of Eq. (41) are -50.5 and -78.7. For this case the orbits were found stable for all the values of γ considered.

The numerical and theoretical results are in excellent agreement when the linearized theoretical model is valid. However, when B_s^{ex} and B_o have opposite signs and $|B_s^{ex}| > |B_o|$, the toroidal field vanishes at some radial distance and the field lines form magnetic cusps. In this case the linear theory does not properly describe the fields and the predictions of the theory are not in agreement with the numerical results.

When

$$\left[\omega_o^2\ \omega_w^2 / (\omega_w - \frac{\Omega_A}{\gamma})^2\ (\frac{\Omega_A^2}{\gamma^2})\right] \ll 1 ,$$

Equation (40) gives

$$\omega_{\pm}^2 = \begin{cases} (\omega_w/2)^2 \left[1 + \dfrac{\omega_o^2}{(\omega_w - \Omega_A/\gamma)(\Omega_A/\gamma)}\right], & \text{(slow mode)} \\ -\dfrac{\omega_w^2}{4} + \dfrac{\Omega_A^2}{\gamma^2} - \omega_w \dfrac{\Omega_\theta}{\gamma} - \dfrac{\omega_o^2\ \omega_w^2}{4(\omega_w - \Omega_A/\gamma)(\Omega_A/\gamma)} . & \text{(fast mode)} \end{cases}$$

In the laboratory frame the slow mode Ω_+ becomes

$$\Omega_+ = \omega_+ - \frac{\omega_w}{2} = \frac{\omega_o^2}{4(1 - \frac{\Omega_A}{\gamma\omega_w})(\frac{\Omega_A}{\gamma})} \quad . \tag{43}$$

The particular solution of Eq. (38) in the rotating frame, for $\dot{\gamma} = 0$ and $\omega_\perp^2$ small, is $\tilde{\psi}_p = \tilde{R}_p + i\tilde{Z}_p$

where

$$\tilde{R}_p = \frac{4\lambda^2(\omega_w - \Omega_A/\gamma + \omega_o/2)}{\omega_o^2\ \omega_w} \cos(\frac{\omega_w t}{2}) \quad , \tag{44}$$

and

$$\tilde{Z}_p = \frac{4\lambda^2(\omega_w - \Omega_A/\gamma - \omega_o/2)}{\omega_o^2\ \omega_w} \sin(\frac{\omega_w t}{2}) \quad . \tag{45}$$

Transforming back to the laboratory frame using the transformation $\psi = \tilde{\psi}\, e^{-i\omega_w t/2}$, we find that the particle orbit is displaced along the horizontal axis by

$$\Delta r = \frac{4\lambda^2}{\omega_o^2\ \gamma^{1/2}} (1 - \Omega_A/\gamma\omega_w) \quad . \tag{46}$$

Figure 14 shows the projection of the particle orbit in the tranverse plane for

$\gamma = 11$, $\varepsilon_t = -0.4$ $B_A = 11KG$, $\omega_w = 6 \times 10^9\ sec^{-1}$, $r_o = 100cm$, $B_{z0} = 118$ G and $v_A \simeq c$. For these parameters Eq. (43) gives a slow

period $\tau_+ = 2\pi/\Omega_+ = 62$ nsec. For the same parameters the code gives $\tau_+ = 60$nsec.

In addition, Eq. (46) gives a displacement $\Delta r = 1.74$ cm , which is identical to the orbit displacement of Fig. 14.

Let's now return to discuss briefly the results of Fig. 10. For the parameters of the run, Eq. (42) gives $\gamma_+ \approx 121$ and $\gamma_- = 65$. When the γ of the particle reaches 65 i.e., at about 300 nsec, it becomes unstable and strikes the wall in one revolution.

In addition, at t=0 the ratio $\Omega_\beta/\omega_w\gamma = 6.67$ and according to Eq. (46) the orbit displacement is negative. As γ increases $\Omega_\beta/\gamma\omega_w$ is reduced and when $\Omega_\beta/\gamma\omega_w < 1$ the orbit dispacement becomes positive. At $\gamma = 46.6$, $\Omega_\beta/\gamma\omega_w \approx 1$ and $\Delta r = 0$. According to Fig. 10b this occurs at $t \approx 210$ nsec , which corresponds to $\gamma \approx 47$ (see Fig. 10c).

V. Self Fields

An accurate self consistent determination of self fields of a high current electron ring confined in a rebatron is difficult, because the minor cross section of the ring has, in general, a complex shape that varies along the toroidal direction.

Since we are interested in the macroscopic motion of the ring and therefore on the self fields that act on the ring centroid, we assume that the ring has a circular cross section and its particle density is uniform. Neglecting toroidal corrections, the fields at the center of the beam, which is located at the distance $(r - r_o)$ and z from the minor axis are[18,26]

$$E_r^s = -2\pi|e|\, n_o r_o \frac{r_b^2}{a^2} \frac{(r - r_o)}{r_o} \tag{47}$$

$$E_z^s = -2\pi|e|\, n_o r_o \frac{r_b^2}{a^2} \frac{z}{r_o} , \tag{48}$$

$$B_r^s = 2\pi|e|n_o\beta_o r_o \frac{r_b^2}{a^2} \frac{z}{r_o} , \tag{49}$$

and

$$B_z^s = 2\pi|e|n_o\beta_o r_o \frac{r_b^2}{a^2} \frac{(r - r_o)}{r_o} , \tag{50}$$

where n_o is the particle density, r_b the beam radius and a the minor radius of the perfectly conducting torus.

When $\dot{\gamma} = 0$, $n = 1/2$ and the beam energy is matched to the vertical field, the equation describing the beam centroid motion in the tranverse rotating plane is given by

$$\ddot{\tilde{\psi}} + \hat{f}_1 \tilde{\psi} + f_3\tilde{\psi}^* - if_2\dot{\tilde{\psi}} = \lambda^2 e^{i\omega_w t/2} , \tag{51}$$

where f_2 and f_3 have been defined under Eq. (38) and

$$\hat{f}_1 = \hat{\omega}_\perp^2 - (\frac{\omega_w}{2})^2 + \frac{\omega_w}{2}\frac{\Omega_a}{\gamma} , \tag{52}$$

where

$$\hat{\omega}_\perp^2 = \frac{v_a^2}{2r_o^2} - \frac{\omega_b^2}{2\gamma^3}(\frac{r_b}{a})^2 , \tag{53}$$

and $\omega_b^2 = 4\pi e^2 n_o/m$.

The solution of Eq. (51) when $\lambda^2 = 0$ is $\tilde{\psi} = \sum_i \tilde{\psi}_{oi} e^{i\omega_i t}$,

where

$$\omega_{\pm}^2 = 1/4(\omega_w - \frac{\Omega_\theta}{\gamma})^2 + (\frac{\Omega_\theta^2}{4\gamma^2} + \hat{\omega}_\perp^2)$$

$$\pm\left[(\omega_w - \frac{\Omega_\theta}{\gamma})^2 (\frac{\Omega_\theta^2}{4\gamma^2} + \hat{\omega}_\perp^2) + \frac{\omega_o^2 \omega_w^2}{4}\right]^{1/2} . \qquad (54)$$

The orbits are stable provided

$$\frac{\Omega_\theta^2}{4\gamma^2} + \hat{\omega}_\perp^2 > 0 \quad , \qquad (55)$$

and

$$\left[\hat{\omega}_\perp^2 - (\frac{\omega_w}{2})^2 + \frac{\omega_w}{2} \frac{\Omega_\theta}{\gamma}\right]^2 - \frac{\omega_o^2 \omega_w^2}{4} > 0 \quad . \qquad (56)$$

Equation (56) can be written as

$$\hat{u} = \hat{\omega}_\perp^4 + 2\hat{\omega}_\perp^2 (\frac{\omega_\omega}{2})(\frac{\Omega_\theta}{\gamma} - \frac{\omega_w}{2}) + (\frac{\omega_w}{2})^2\left[(\frac{\Omega_\theta}{\gamma} - \frac{\omega_w}{2})^2 - \omega_o^2 \right] > 0 \quad , \qquad (57)$$

and its roots are given by

$$\frac{\hat{\omega}_{\perp\pm}^2}{(\omega_w/2)} = -\left[(\frac{\Omega_\theta}{\gamma} - \frac{\omega}{2}^w) \pm \omega_o \right] . \qquad (58)$$

When $\left|(\frac{\Omega_\theta}{\gamma} - \frac{\omega_w}{2})\right| > \left|\omega_o\right|$, the two roots of inequality (57) are both either positive or negative depending upon the sign of $(\frac{\Omega_\theta}{\gamma} - \frac{\omega_w}{2})$ and ω_o . The results are summarized in Table V.

For $\gamma >> 1$, Eq. (58) becomes

$$\hat{\omega}_{\perp\pm}^2 = (\omega_w/2)^2, \qquad (59)$$

i.e. the orbits are always stable provided inequality (55) is satisfied.

The maximum amount of space charge that can be confined by a rebatron can be determined from Eq. (55). When

$$v_\theta^2/2r_o^2 \ll (\frac{\omega_b^2}{2\gamma^3})(\frac{r_b}{a})^2 ,$$

Eq. (55) gives

$$\frac{\nu}{\gamma} < \frac{\Omega_\theta^2 a^2}{8c^2} . \qquad (60)$$

For a = 10 cm, B_θ = 10 KG, γ = 7, Eq. (60) gives $\nu \approx 3{,}000$ or I ≈ 50 MA.

When the current of the beam is large, $\hat{\omega}_l^2 \ll 0$. However, as γ increases $\hat{\omega}_l^2$ approaches it asymptotic value $v_\theta^2/2r_o^2$. Similarly, the two roots $\hat{\omega}_{l\pm}^2$ approach their asymptotic value given by Eq. (59).

Figure 15 shows the stability diagram at t = 0, when $(\frac{\Omega_\theta}{\gamma} - \frac{\omega_w}{2}) < 0$ and $\omega_o < 0$. For this case the stability condition is $-\frac{\omega_w}{2}\left[(\frac{\Omega_\theta}{\gamma} - \frac{\omega_w}{2})\right] + \frac{\omega_o\omega_w}{2} > \hat{\omega}_l^2 > -\frac{\Omega_\theta^2}{4\gamma^2}$.

During acceleration γ increases and therefore both $-\Omega_\theta^2/4\gamma^2$ and $\hat{\omega}_l^2$ move to the right of the diagram. Therefore, it may be argued that before $\hat{\omega}_l^2$ crosses the vertical axis, $-\Omega_\theta^2/4\gamma^2$ catches up with it and the ring becomes unstable. A similar situation would occurs when $\hat{\omega}_l^2$ becomes equal to $\hat{\omega}_{l+}^2$. However, we have shown that when the system is stable at t = 0 it will remain stable for any γ that exceeds the initial γ.

VI. Conclusions

We have carried out an extensive numerical and analytical investigation of the beam dynamics in a rebatron accelerator. Although the analytical work is based on simple, linear approximations for the various fields, the two approaches give very similar results when these approximations are valid.

Our studies indicate that when self field effects can be ignored, the particle normalized energy can be increased from $\gamma = 7$ to $\gamma \approx 70$, at constant betatron field, before confinement is lost. This implies that the device has a bandwidth that approaches 1000%. This bandwidth can be further increased by increasing the current in the torsatron wires.

Even in the absence of the space charge, there is a range of parameters [see Eq. (42)] for which the rebatron is unstable. However, this orbit instability can be easily avoided by a judicious choice of the various parameters.

As far as orbit stability is concerned, the maximum electron beam current that can be confined in a rebatron accelerator is given by Eq. (60) and is impressively high. Therefore, it is expected that the limiting beam current in a rebatron would be determined from collective instabilities and not from the macroscopic stability of beam orbits.

Although the bandwidth of rebatron accelerators is very high, the maximum energy that can be obtained by these devices, with time independent magnetic fields, is rather limited. To achieve very high energies ($\gamma > 1000$) the betatron magnetic field should be replaced by a local vertical magnetic field that varies rapidly with time and approximately in synchronism with the beam energy. Such a fast vertical field can be generated by two coaxial, cylindrical lines that carry

current in the opposite direction. The axes of these lines coincide with the major axis of the toroidal vessel and they are located symmetrically around the minor axis of the torus. These transmission lines change mainly the local vertical magnetic field, while the magnetic flux through the beam orbit remains approximately constant. The mismatch between the beam energy and the vertical field is alleviated by the strong focusing field. The effect of the rapidly varying vertical magnetic field on the beam dynamics will be reported in a forthcoming publication.

Table I

Parameters relevant to the torsatron fields shown in Fig. 3. Only two terms retained in the series of Eqs. (1) to (3).

Torus major radius	r_o (cm)	= 100
Windings minor radius	ρ_o (cm)	= 12
Toroidal chamber minor radius a (cm)		= 10
$\alpha = 2\pi/L$ (cm^{-1})		= 0.1
Field Strength Factor	ε_t	= 0.2
Winding Current I(kA)		= 62.37
	ℓ	= 2
Additional Toroidal Field	B_s^{ex} (kG)	= - 6

Table II

Parameters of the run shown in Fig. 6

Torus Major Radius r_o(cm)		= 100
Winding Minor Radius ρ_o (cm)		= 12
Toroidal Chamber Minor Radius a(cm)		= 10
$\alpha = 2\pi/L$ (cm^{-1})		= 0.1
Field Strength Factor	ε_t	= 0
Winding Current I (kA)		= 0
	ℓ	= 2
Additional Toroidal Field	B_s^{ex}(kG)	= -6
Betatron Field	B_{zo} (G)	= 118
Ext. Field Index	n	= 0.5
Initial	γ	= 7.0
Initial Positions	$\rho = \phi = s$	= 0
Initial Velocities	$v_\rho = v_\phi = 0$, $v_s = c$	

Table III

Parameters of the run shown in Fig. 7.

Torus Major Radius r_o(cm)	= 100
Winding Minor Radius ρ_o (cm)	= 12
Toroidal Chamber Minor Radius a(cm)	= 10
$\alpha = 2\pi/L$ (cm^{-1})	= 0.1
Field Strength Factor ε_t	= - 0.4
Winding Current I (kA)	=-124.7
ℓ	= 2
Additional Toroidal Field B_s^{ex} (kG)	= - 6
Betatron Field B_{zo}(G)	= 118
Ext. Field Index n	= 0.5
Initial γ	= 7.0
Initial Positions $\rho = \phi = s$	= 0
Initial Velocities $v_\rho = v_\phi = 0$, $v_s \approx c$	

Table IV

Parameters of the run shown in Fig. 8.

Torus Major Radius r_o(cm)	= 100
Winding Minor Radius ρ_o(cm)	= 12
Torodial Chamber Minor Radius a(cm)	= 10
$\alpha = 2\pi/L$ (cm^{-1})	= 0.1
Field Strength Factor ε_t	= -0.8
Winding Current I (kA)	= -250
ℓ	= 2
Additional Torodial Field B_s^{ex}(kG)	= -6
Betatron Field B_{zo}(G)	= 118
Ext. Field Index n	= 0.5
Initial γ	= 7.0
Initial Positions $\rho = \phi = s$	= 0
Initial Velocities $v_\rho = v_\phi = 0$, $v_s \approx$	c

Table V

Roots of inequality (57) as given by Eq. (58), when $\left|\left(\frac{\Omega_\theta}{\gamma} - \frac{\omega_w}{2}\right)\right| > \left|\omega_o\right|$.

$\left(\frac{\Omega_\theta}{\gamma} - \frac{\omega_w}{2}\right)$	ω_o	$2\hat{\omega}^2_{1,\pm}/\omega_w$
+	+	both negative
-	-	both positive
-	+	both positive
+	-	both negative

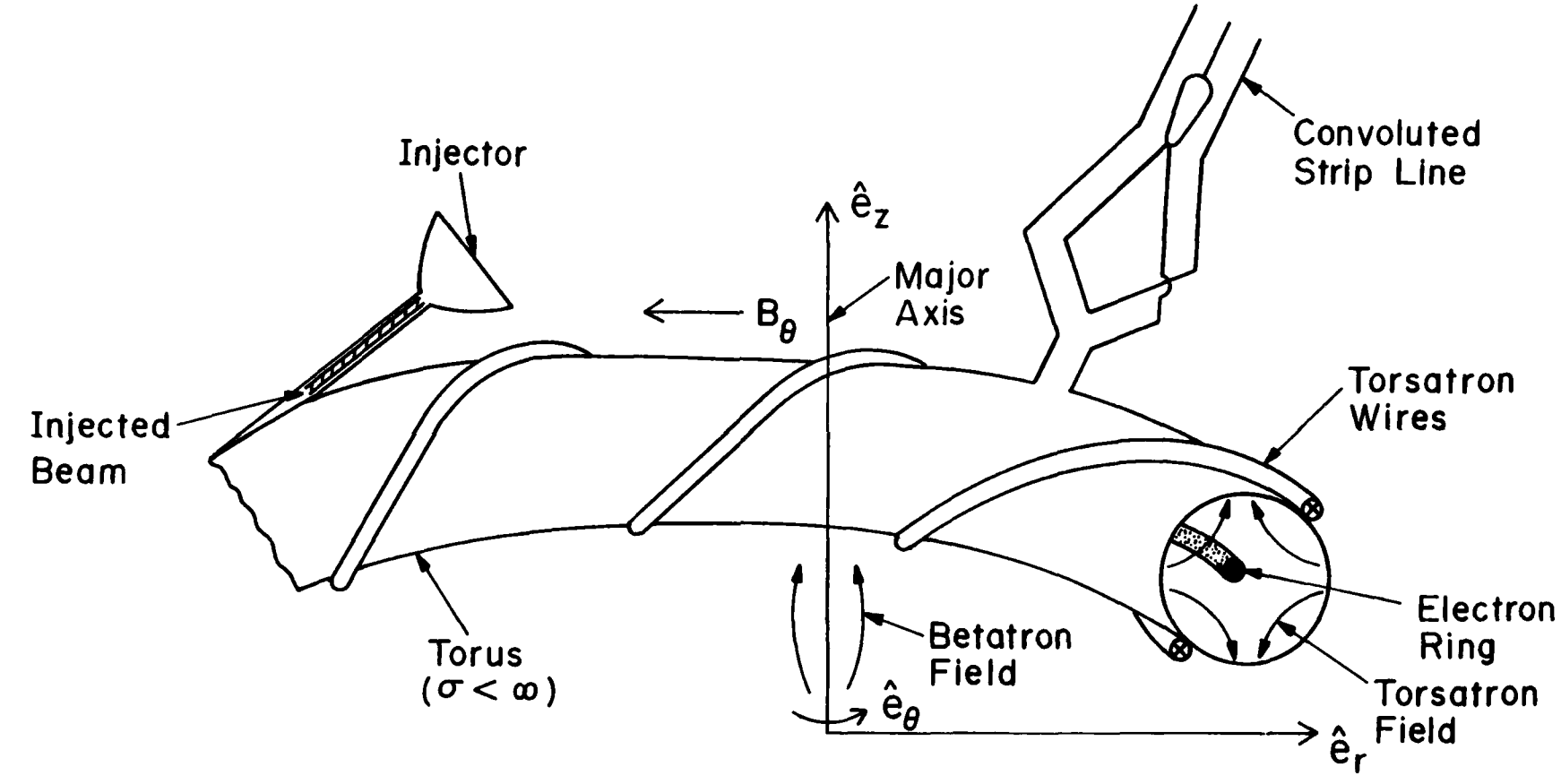

Fig. 1 — Schematic of a rebatron. The accelerating gap is energized by two or more transmission lines that are symmetrically distributed around the minor axis.

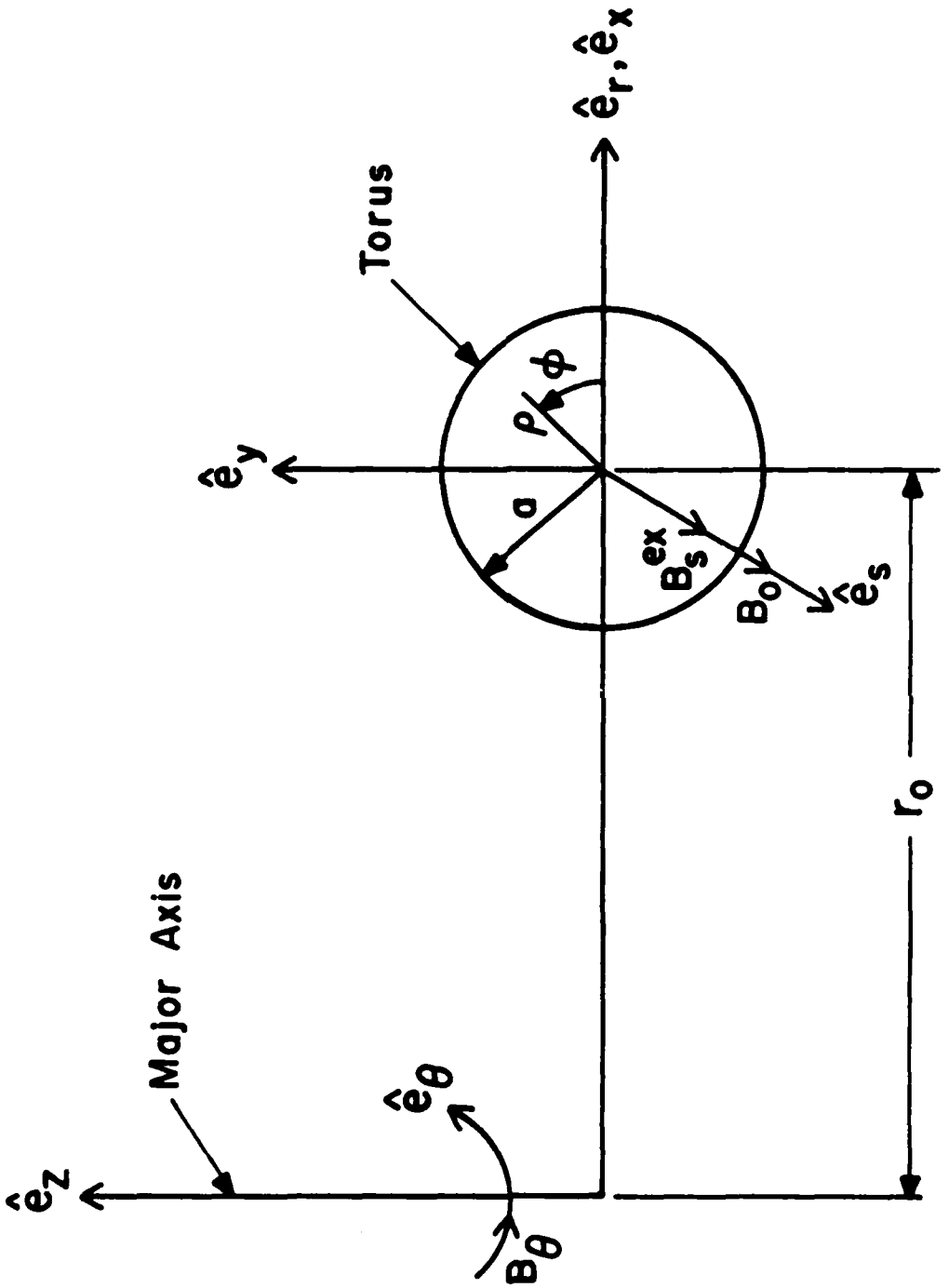

Fig. 2 — Systems of coordinates

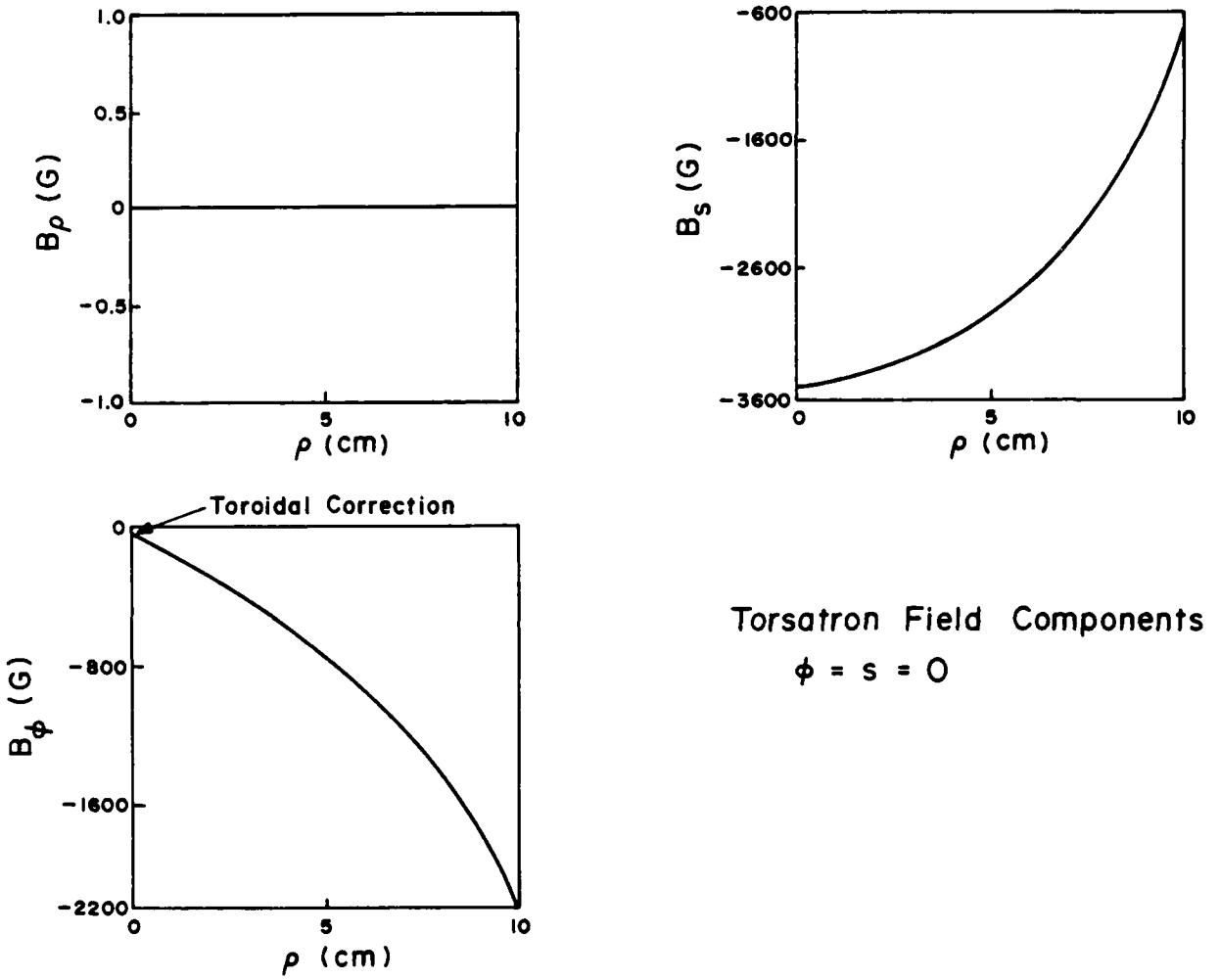

Fig. 3 — Torsatron magnetic field components (a) at ϕ = s = 0 and (b) at s = 0, $\phi = \pi/2$. In addition to the torsatron field there is toroidal field $B_s^{ex} = -6$ kG that is produced by a set of toroidal coils. (c) magnetic field lines in r, z and ρ, s planes.

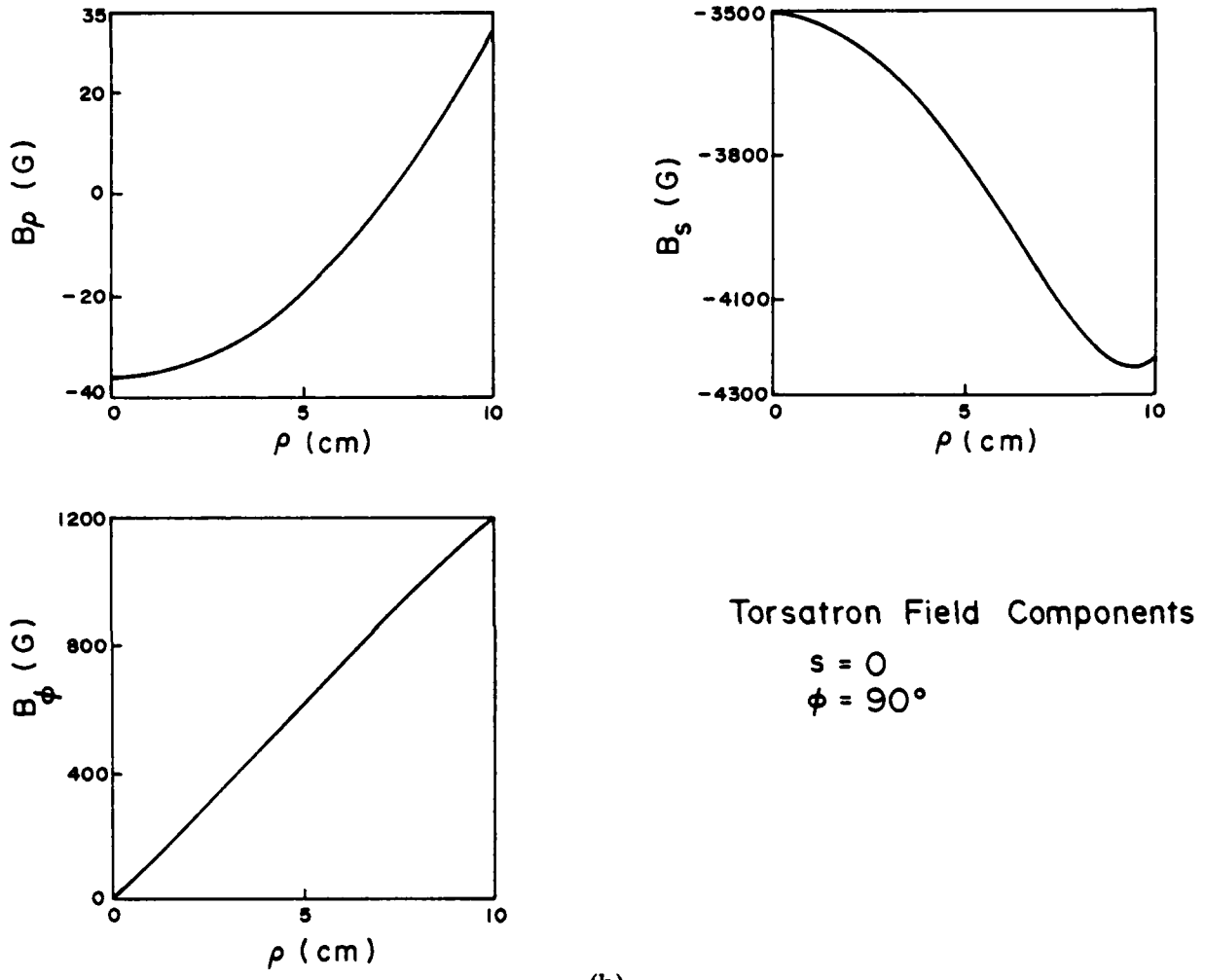

(b)

Fig. 3 (Cont'd) — Torsatron magnetic field components (a) at ϕ = s = 0 and (b) at s = 0, $\phi = \pi/2$. In addition to the torsatron field there is toroidal field $B_s^{ex} = -6$ kG that is produced by a set of toroidal coils. (c) magnetic field lines in r, z and ρ, s planes.

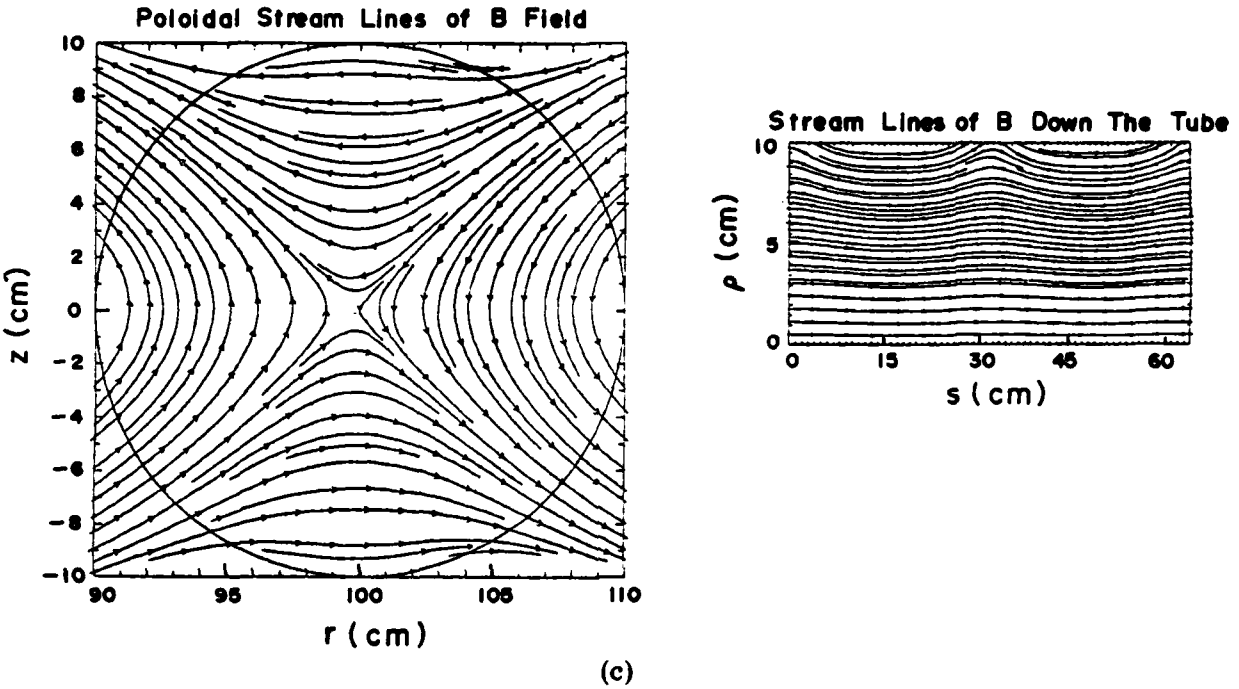

(c)

Fig. 3 (Cont'd) — Torsatron magnetic field components (a) at ϕ = s = 0 and (b) at s = 0, $\phi = \pi/2$. In addition to the torsatron field there is toroidal field $B_s^{ex} = -6$ kG that is produced by a set of toroidal coils. (c) magnetic field lines in r, z and ρ, s planes.

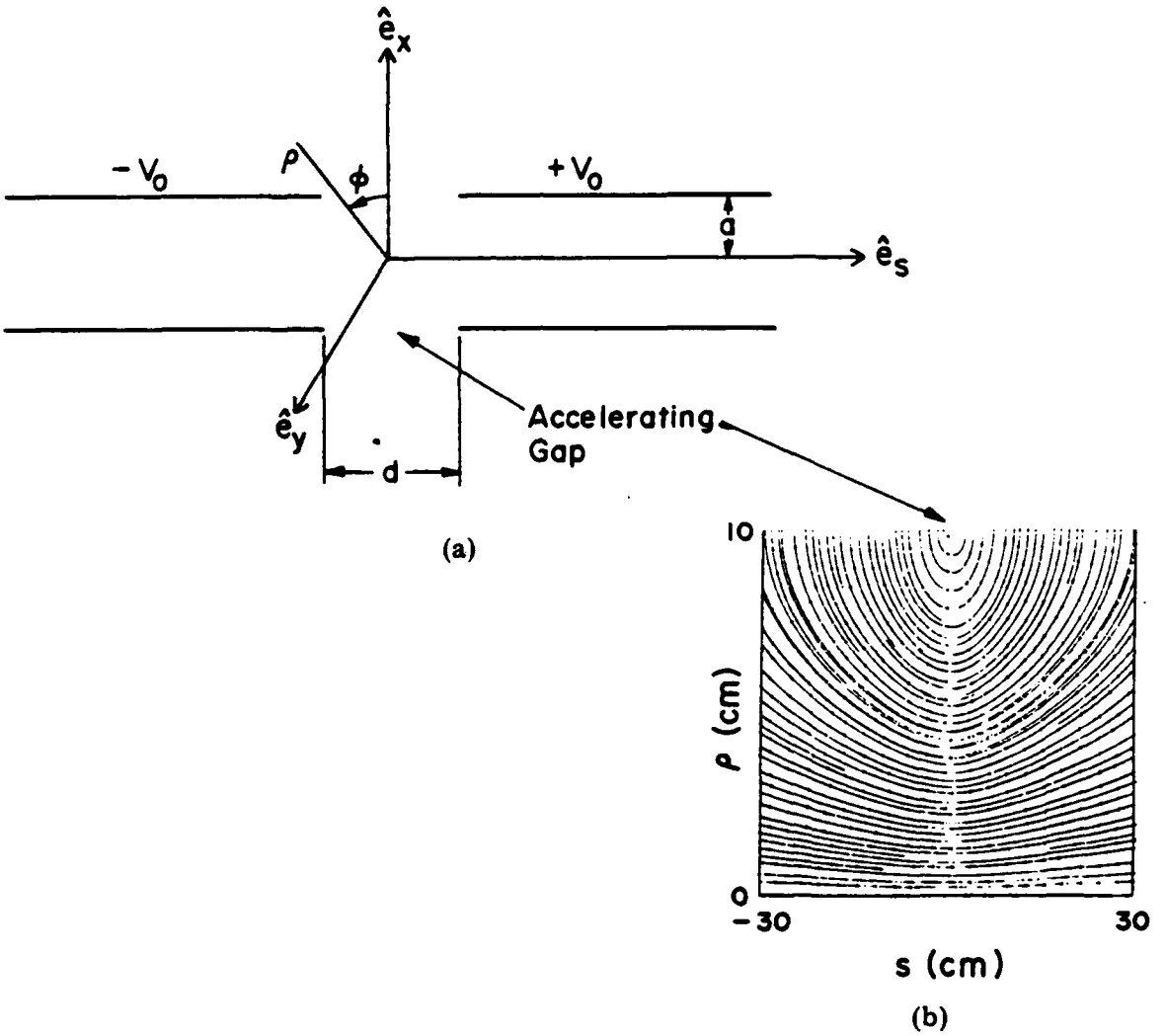

Fig. 4 — (a) Configuration and (b) field lines of the accelerating electric field.

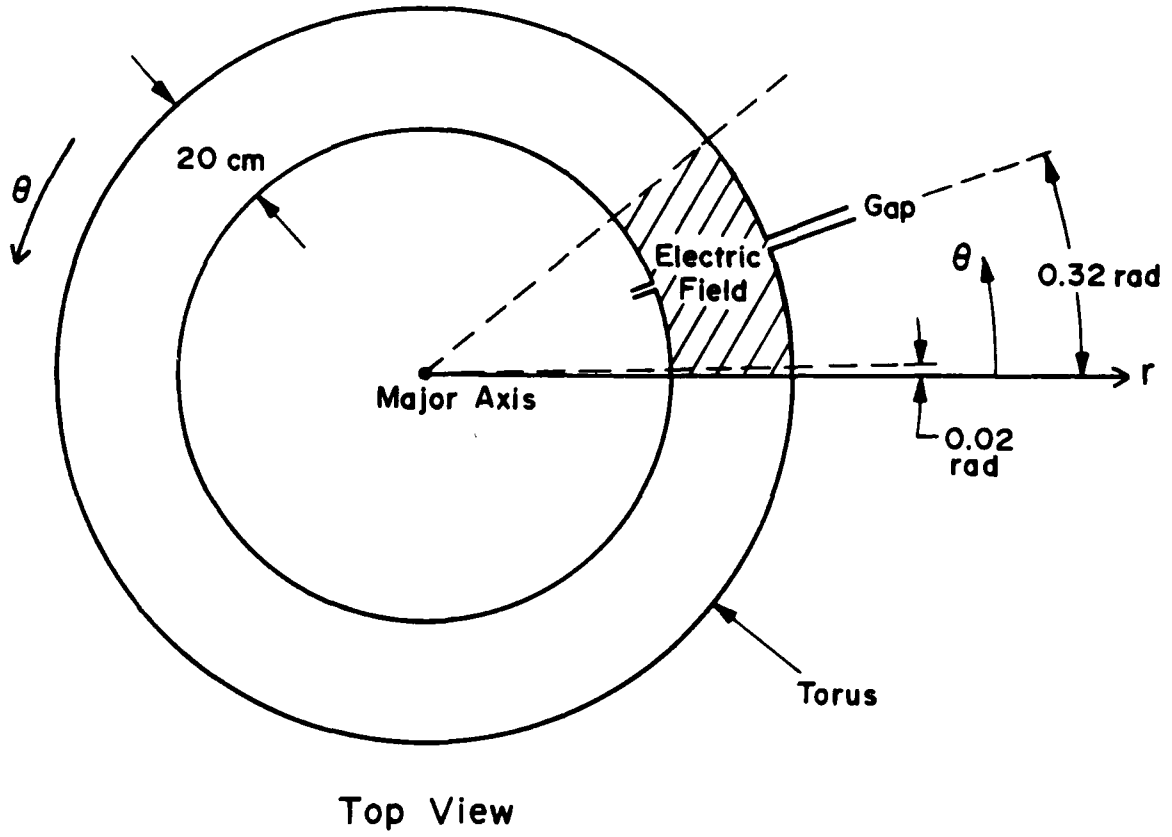

Fig. 5 — Top view of the torus. The accelerating field is limited to ±30cm around the gap.

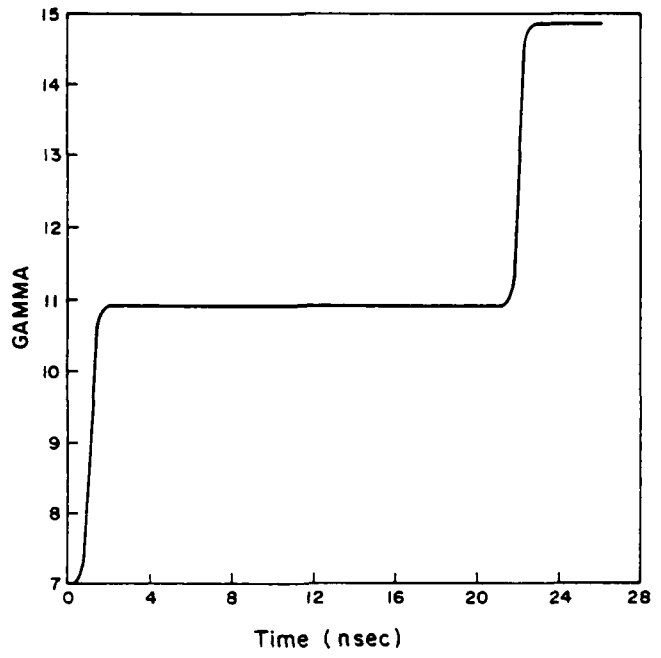

(a)

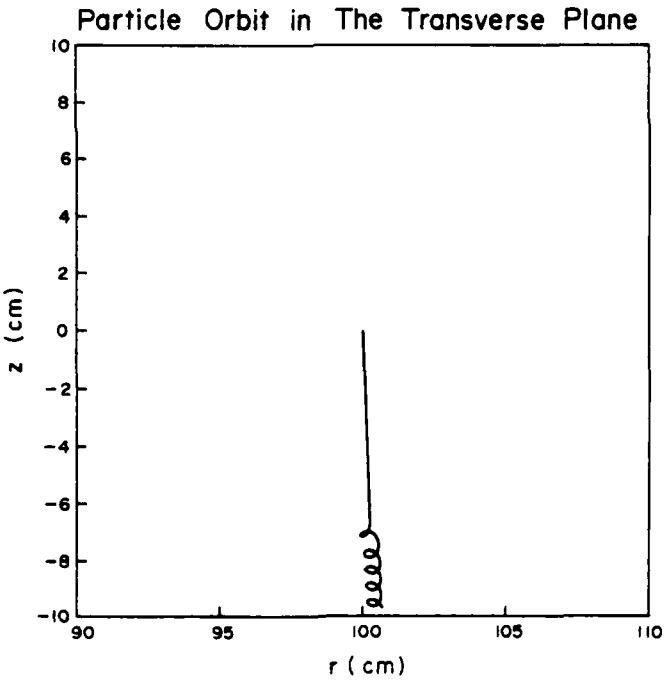

(b)

Fig. 6 — (a) γ of particle as a function of time and (b) particle orbit in the r, z plane in the absence ($\epsilon_t = 0$) of torsatron field. The various parameters for this run are listed in Table II.

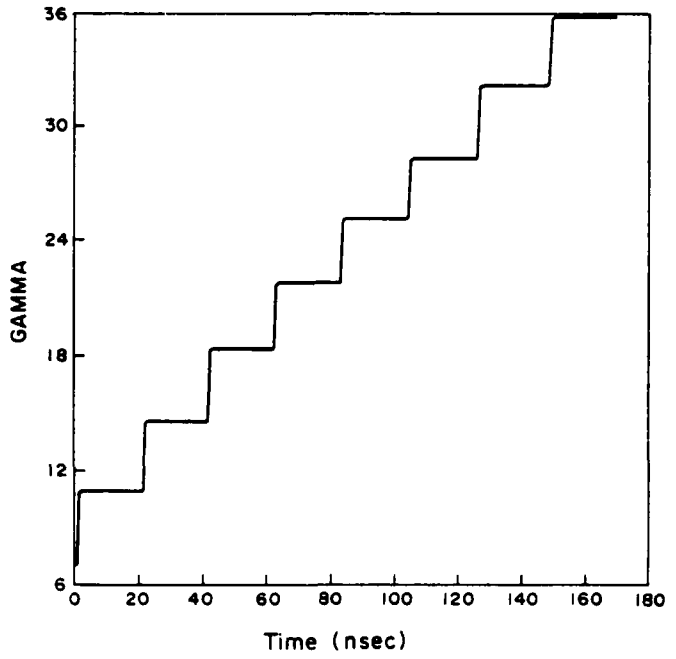

(a)

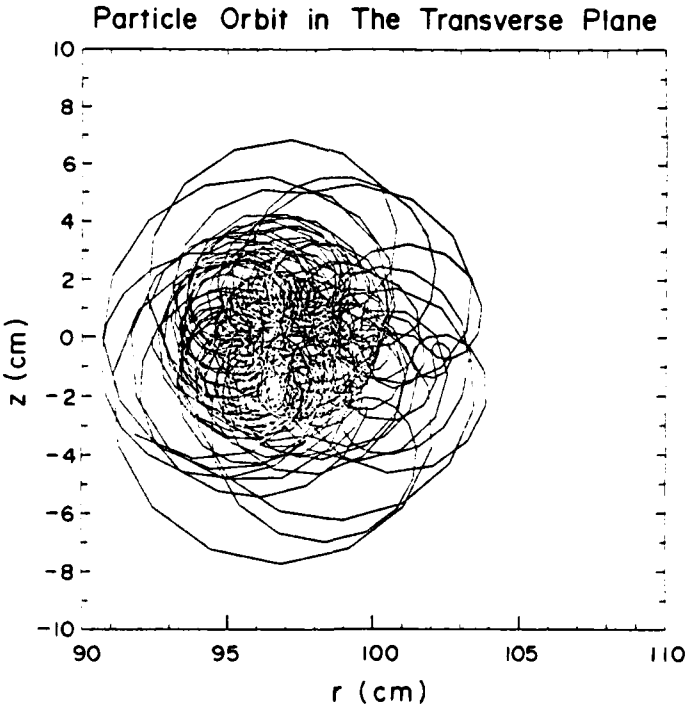

(b)

Fig. 7 — (a) γ of particle as a function of time and (b) particle orbit in the r, z plane for moderate ($\epsilon_t = -0.4$) torsatron field. The various parameters for this run are listed in Table III.

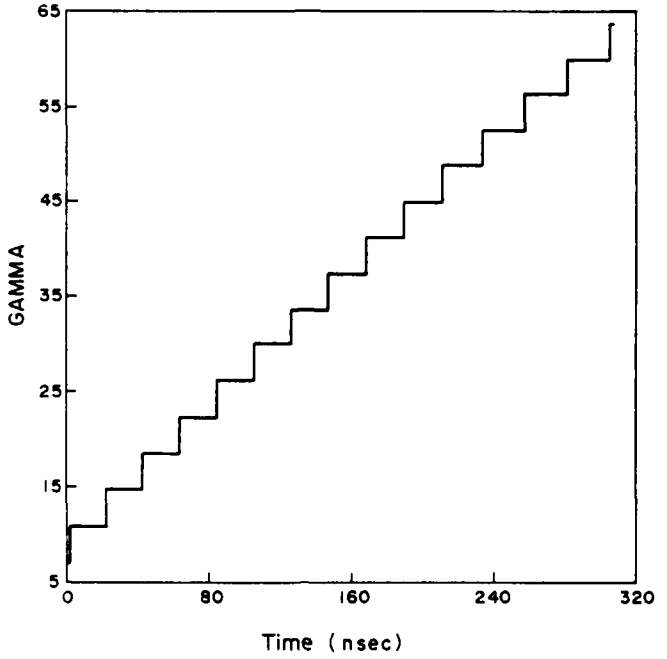

(a)

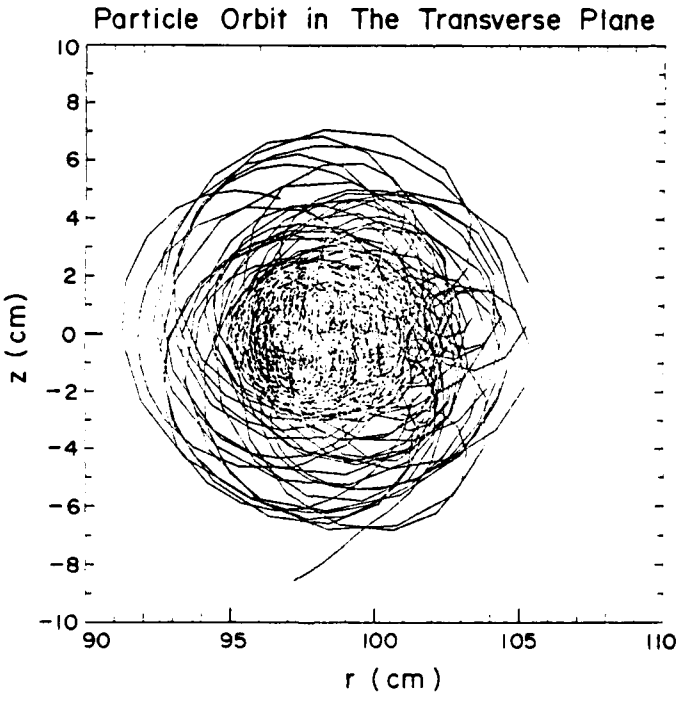

(b)

Fig. 8 — (a) γ of particle as a function of time and (b) particle orbit in the r, z plane for high ($\epsilon_t = -0.8$) torsatron field. The various parameters for this run are listed in Table IV.

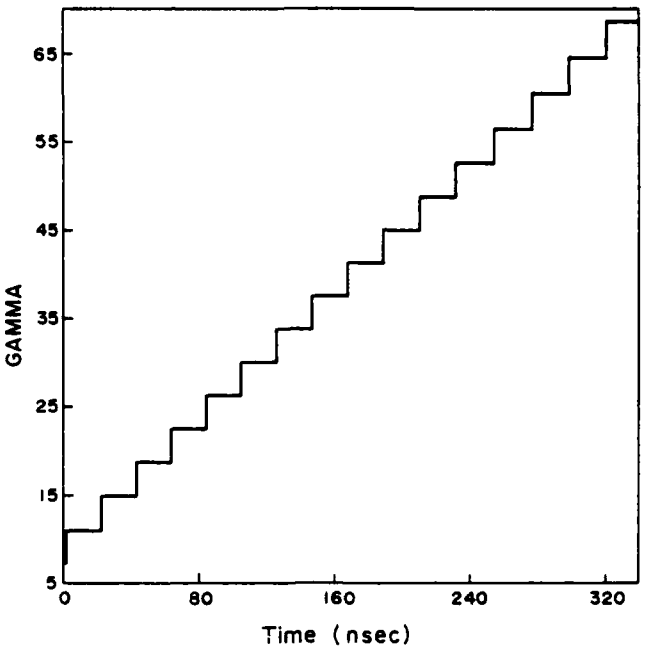

(a)

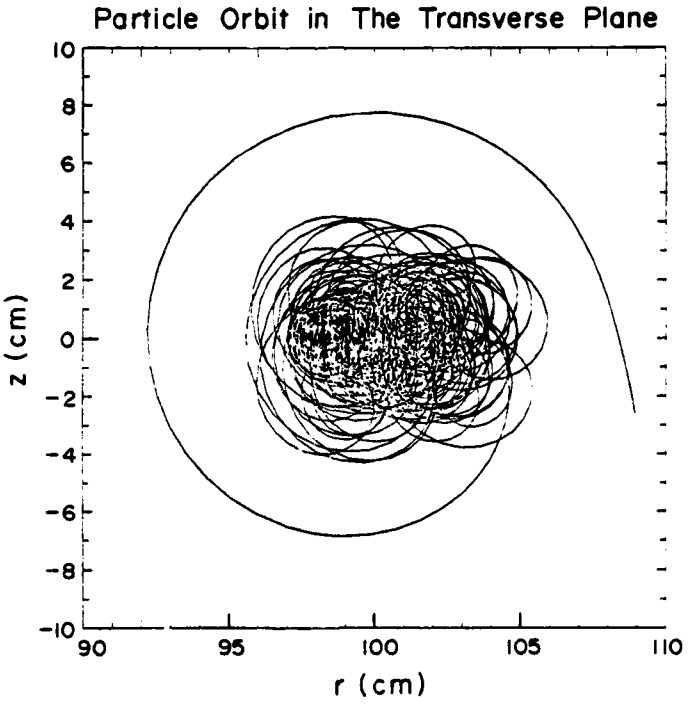

(b)

Fig. 9 — (a) γ of particle as a function of time and (b) particle orbit in the r, z plane for the same parameters as Figure 8 except at a higher betatron field.

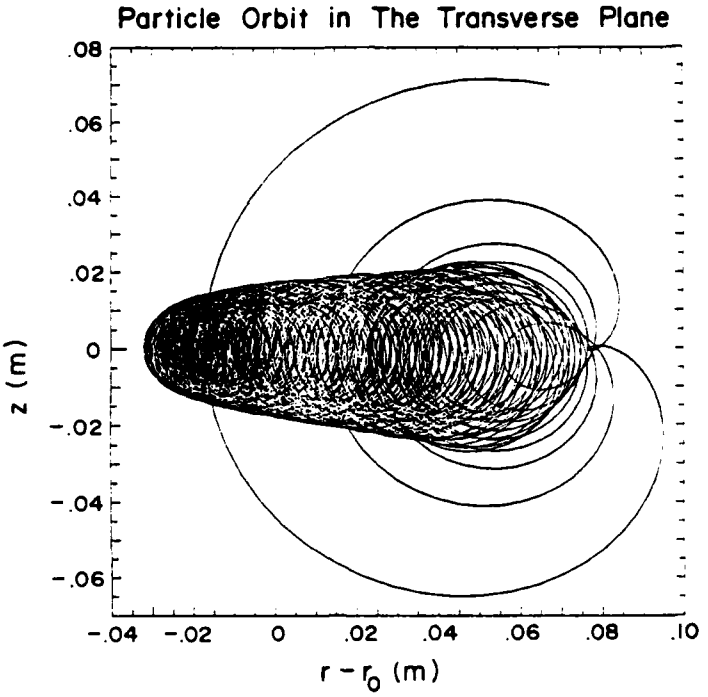

(a)

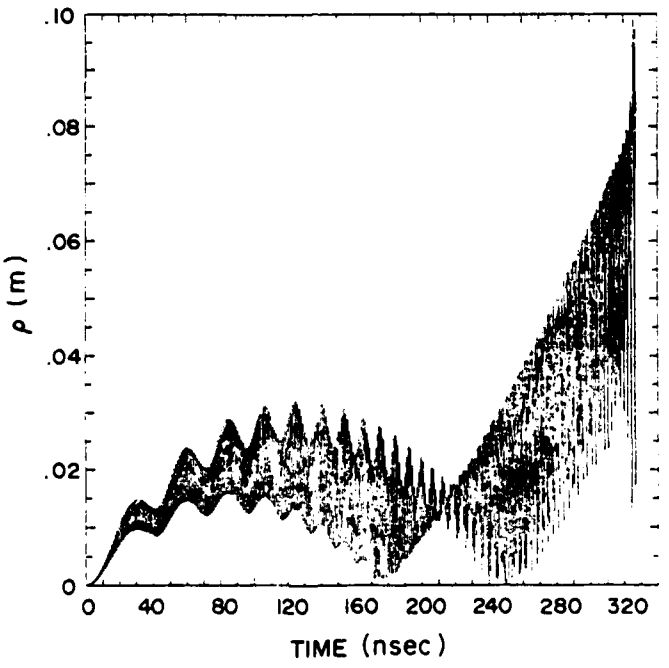

(b)

Fig. 10 — (a) Particle orbit in the r, z plane; (b) particle radius as a function of time and (c) γ of particle as a function of time. These results have been obtained from the linear equations (36) and (37). The results shown are in the Lab. frame. The various parameters for this run are the same with those of Figure 8.

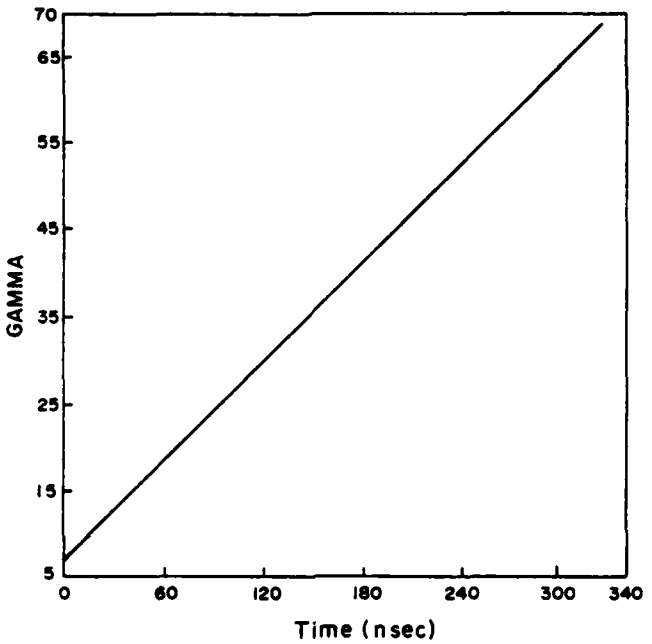

(c)

Fig. 10 (Cont'd) — (a) Particle orbit in the r, z plane; (b) particle radius as a function of time and (c) γ of particle as a function of time. These results have been obtained from the linear equations (36) and (37). The results shown are in the Lab. frame. The various parameters for this run are the same with those of Figure 8.

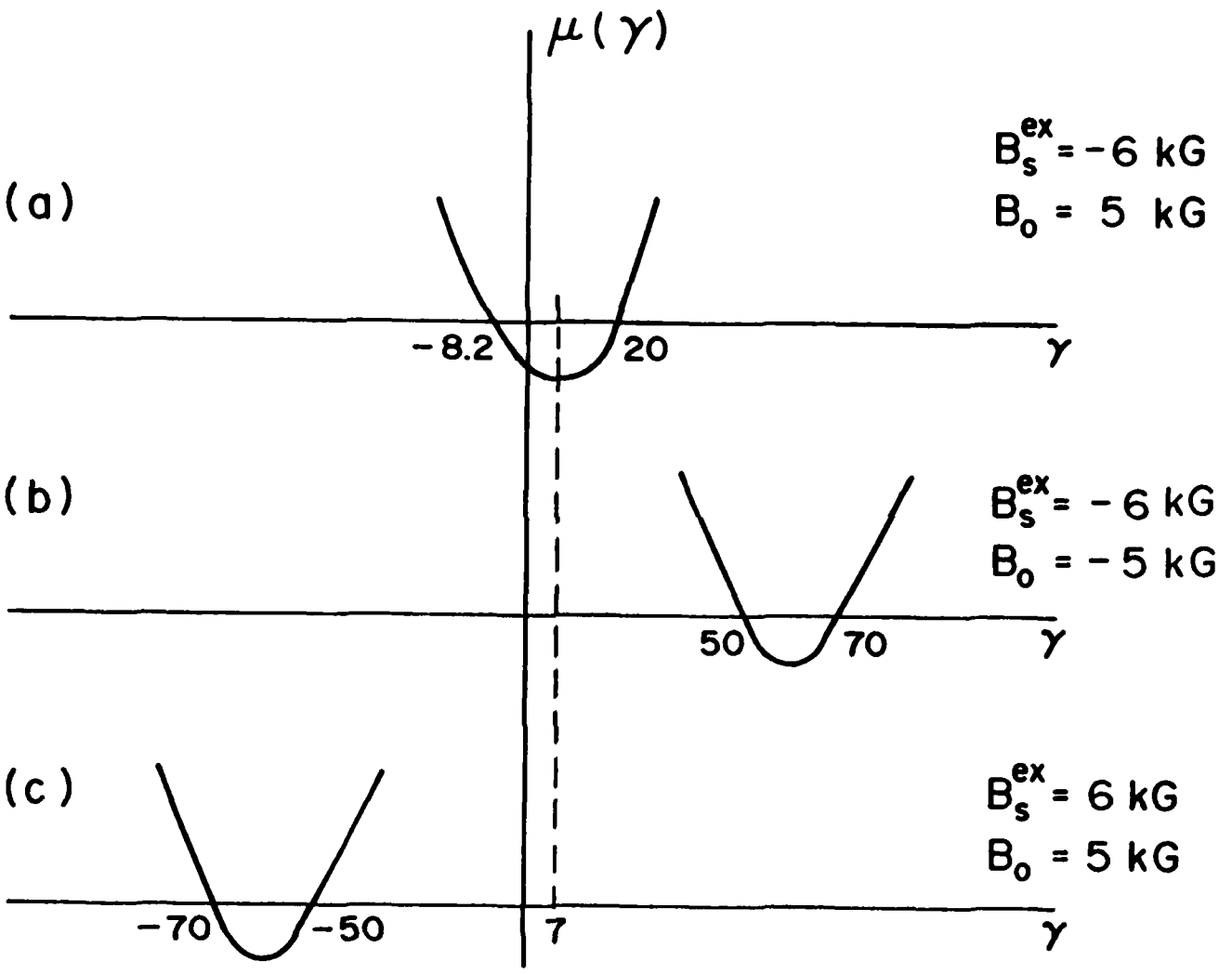

Fig. 11 — Plot of $\mu(\gamma)$ given in Equation (41) for three different combinations of B_s^{ex} and B_o.

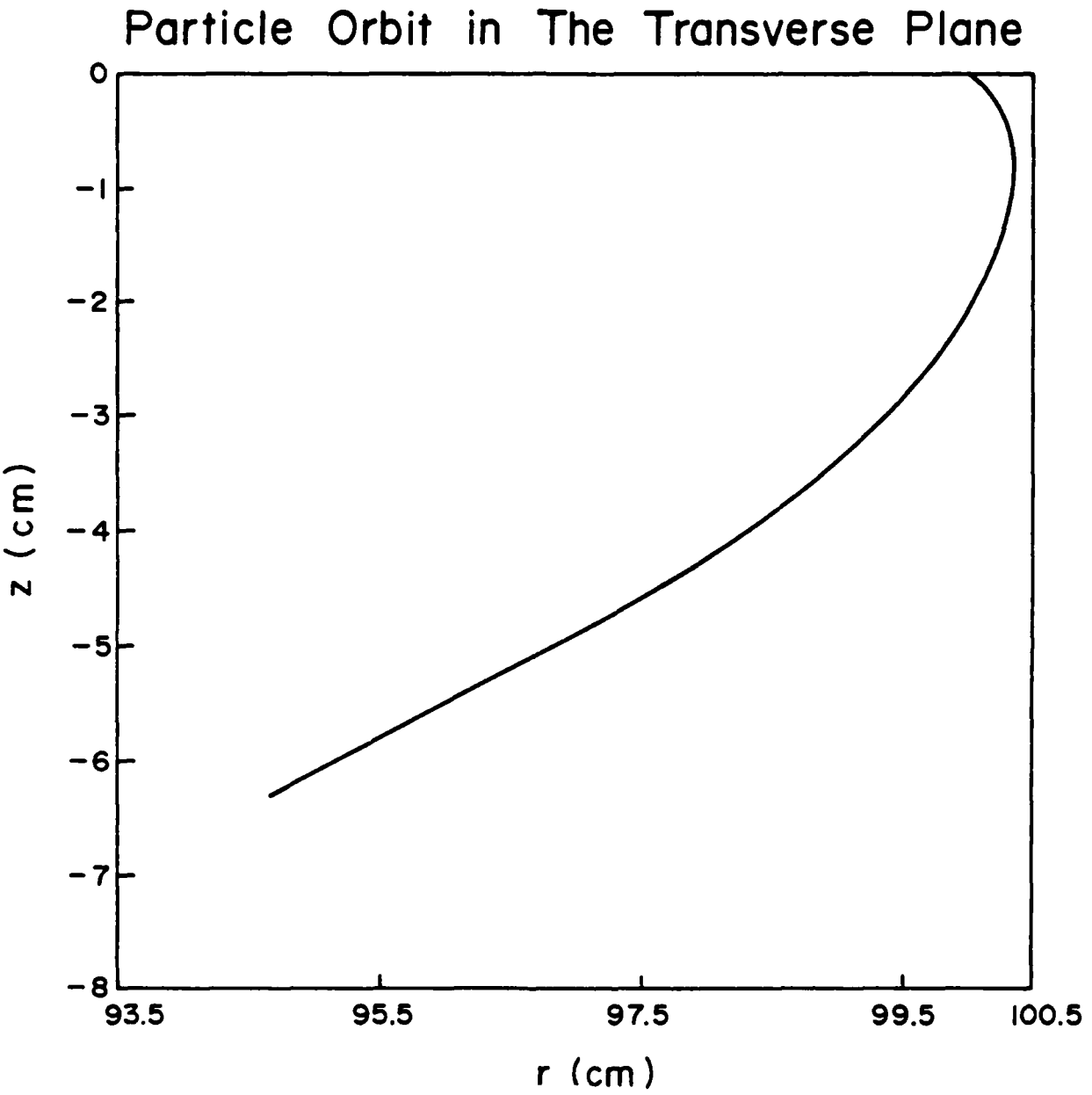

Fig. 12 — Particle orbit in the r, z plane for the same parameters as those in Figure 11a.

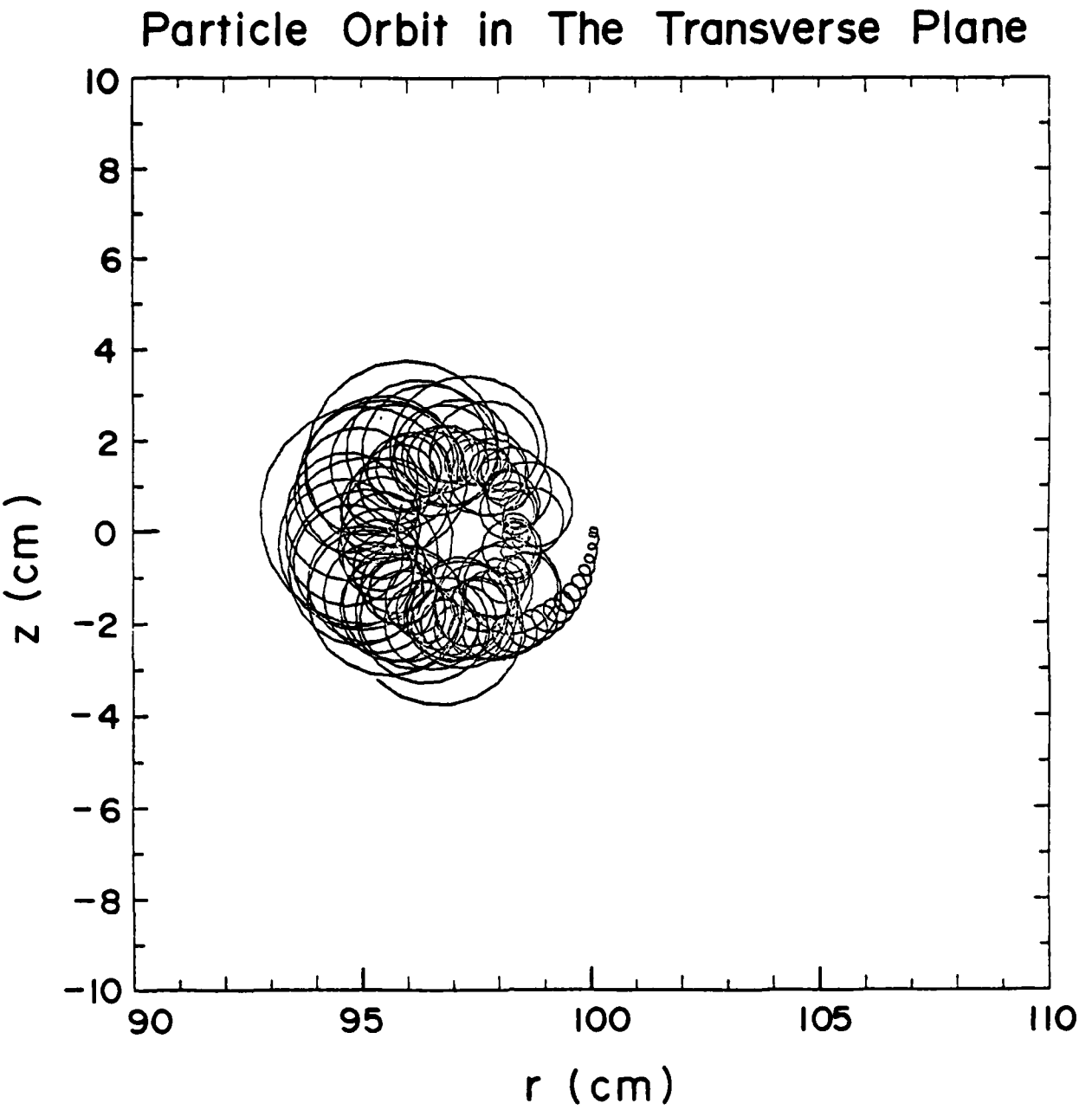

Fig. 13 — Particle orbit in the r, z plane for the same parameters as those in Figure 11b.

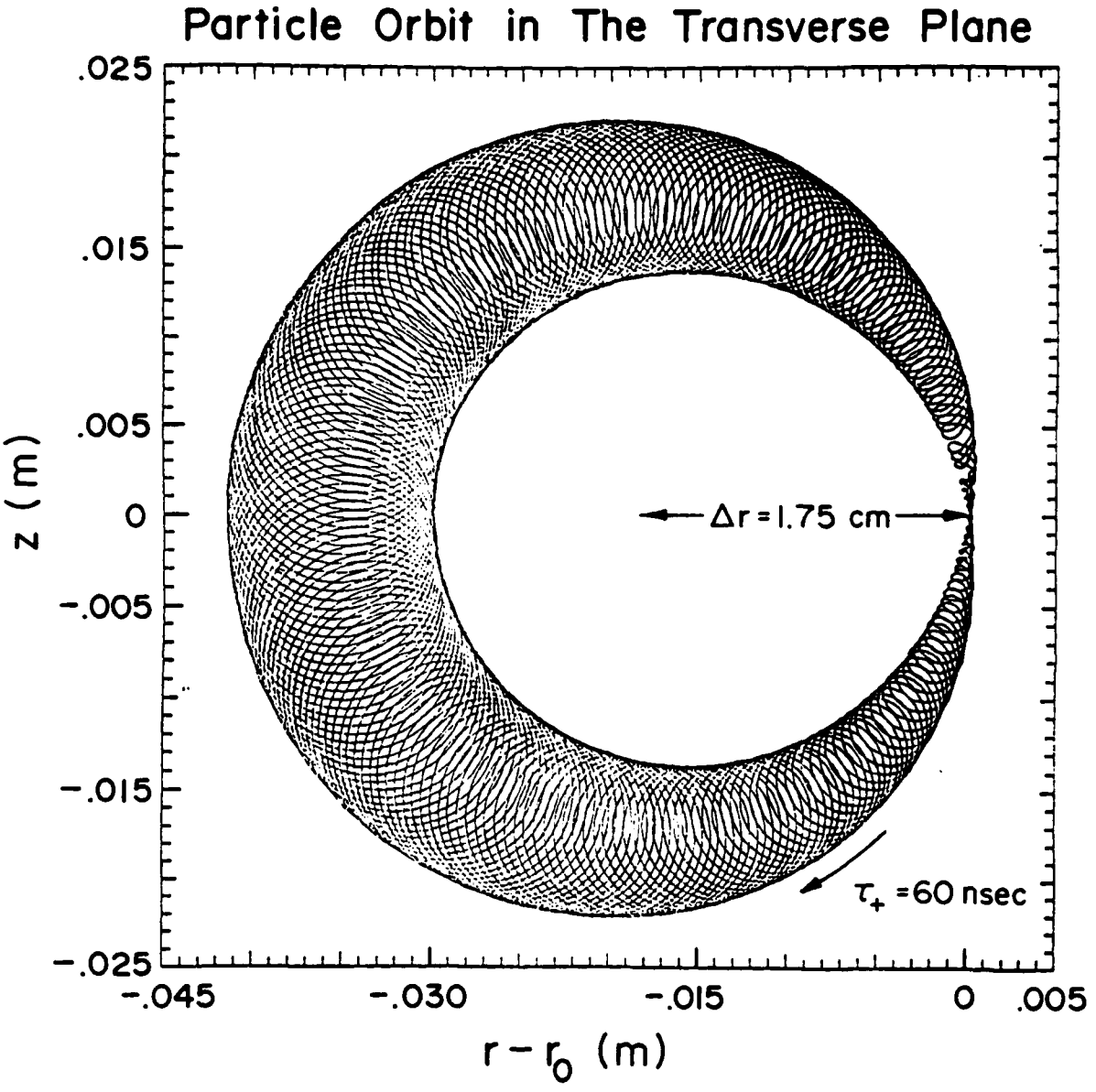

Fig. 14 — Particle orbit in the r, z plane for an initially mismatched beam and $\dot{\gamma} = 0$. The particle rotated around the equilibrium position four times with a period of 60 nsec. The theory [Equation (43)] predicts a period of 62 nsec and the nonlinear equations give similar orbits with a period of about 55 nsec.

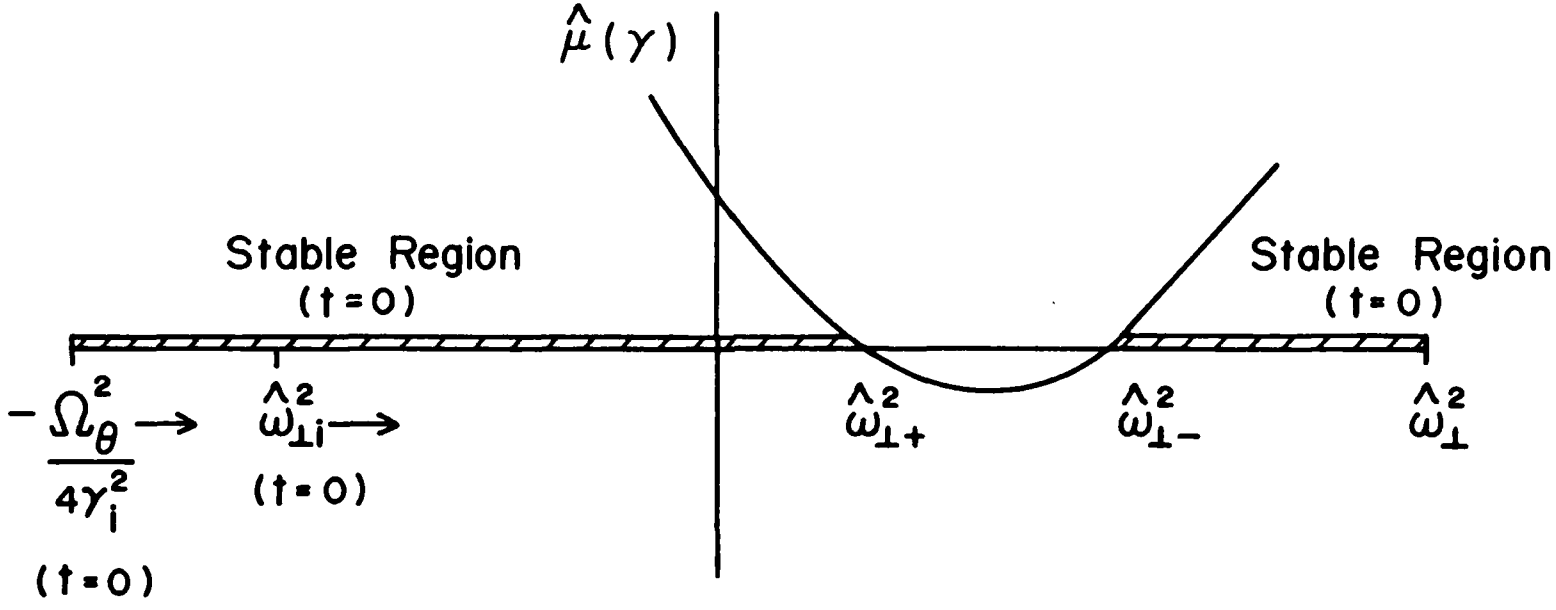

Fig. 15 — Plot of $\hat{\mu}(\gamma)$ of Equation (57) as a function of $\hat{\omega}_\perp^2$. If the system is stable at t = 0, it will remain stable for any γ that exceeds the initial γ.

Acknowledgments

*Work is jointly supported by the Office of Naval Research and U. S. Army Ballistic Research Laboratory, Aberdeen, Md.

(a) Permanent Address: Sachs/Freeman Associates, Bowie, Md. 20715

(b) Permanent Address: Science Applications, Inc., McLean, Va. 22102

References

1. C. A. Kapetanakos and P. Sprangle, Phys. Today, V. 38, #2 (Feb 1985), p. 58.
2. C. A. Kapetanakos and P. Sprangle, NRL Memo Report No. 5259, 1984 AD-A142303.
3. E. T. Gerry and S. A. Mani, W. T. Schafer Associates Report No. DOE/ER-0176 (1983).
4. P. Sprangle and T. Coffey, Phys. Today, V. 36, #12 (Dec 1983).
5. D. Keefe, Part. Acc. 11, 187 (1981).
6. N. C. Christofilos, et al., Rev. Sci. Instrum. 35, 886 (1964).
7. J. E. Leiss, N. J. Norris and M. A. Wilson, Part. Acc. 10, 223 (1980).
8. T. J. Fessenden, et al., Proc. of the Int. Top. Conf. on High-Power Electron and Ion Beam Research and Technology; Palaiseau, France, June 29-July 3, 1981, p. 813. AD-A057 218 Vol I, AD A057 219 Vol. II, March 78, edition.
9. R. J. Briggs, et al., Proc. 1981 Particle Accel. Conf.; IEEE Trans.

Nucl. Sci. NS-28 (June 1981), p. 3360.

10. A. I. Pavlovskii, et al., Sov. Phys. Dokl. 25, 120 (1980).

11. K. R. Prestwich, et al., IEEE Trans. on Nucl. Sci. NS-30, 3155 (1983).

12. L. N. Kazanskii, A. V. Kisletsov and A. N. Lebedev, Atomic Energy 30, 27 (1971).

13. M. Friedman, Appl. Phys. Lett. 41, 419 (1982).

14. D. W. Kerst, Nature 157, 90 (1946).

15. A. I. Pavlovskii, et al., Sov. Phys. Tech. Phys. 22, 218 (1977).

16. P. Sprangle and C. A. Kapetanakos, J. Appl. Phys. 49, 1 (1978).

17. N. Rostoker, Comments on Plasma Physics, Vol. 6, p. 91 (1980).

18. C. A. Kapetanakos, P. Sprangle, D. P. Chernin, S. J. Marsh and I. Haber, Phys. Fluids 26, 1634 (1983).

19. C. W. Roberson, A. Mondelli and D. Chernin, Phys. Rev. Lett. 50, 507 (1983).

20. A. A. Mondelli and C. W. Roberson, Particle Accelerators 15, 221 (1984).

21. P. Sprangle and C. A. Kapetanakos, NRL Memo Report No. 5458 (1984).

22. L. Teng, Argonne Nat. Lab. Report No. ANLAB-55 (1959); G. Salardi, et al., Nucl. Instr. and Methodes 59, 152 (1968); R. M. Pearce, Nucl. Instr. and Methodes 83, 101 (1970); R. L. Gluckstern, Proc. Kinear Accel. Conf., 1979, p. 245.

23. P. A. Politzer, MIT Report No. 77-1 (1977).

24. R. E. Potok, H. Becker, L. Bromberg, D. Cohn, N. Diatchenko, P. B. Roemer and J.E.C. Williams MIT Report PFC/RR-82-10 (1982).

25. I. S. Danilkin, in Stellarators, Proc. of the P.N. Lebeder Inst. (Consultants Bureau, N.Y. 1974) Vol. 65, p. 23. [Note: We have

rederived the toroidal correction and found that two signs in the expression for the potential are different than those given by Danilkin in his Eqs. (24) and (26)].

26. P. Sprangle, C.A. Kapetanakos and S.J. Marsh NRL memo report no. 4666 (1981), (AD-A108359).

END

FILMED

6-85

DTIC